Georeferencing in the Context of Building Information Modelling

Štefan Jaud[a,*], Andreas Donaubauer[b], Otto Heunecke[c], André Borrmann[a,**]

[a] *Chair for Computational Modeling and Simulation, Technical University of Munich, Munich, Germany*

[b] *Chair of Geoinformatics, Technical University of Munich, Munich, Germany*

[c] *Institute of Geodesy, Universität der Bundeswehr München, Munich, Germany*

Abstract

An important element of metadata for any building information modelling (BIM) model is its location and orientation on the Earth. In most cases, engineering design is based on Cartesian coordinate systems. However, as facilities are placed in a geospatial context, discrepancies result from the transformation from the Earth's curved surface to the orthogonal coordinate system and engineers and developers must take this into account. With this in mind, the dimensions of a model may not correspond to those in the real world, but are rather distorted according to the used coordinate reference system (CRS).

We provide a thorough background of geospatial and BIM models to define and illustrate the problem at hand. We introduce three possibilities for spatial interpretation of the geometries and their locations within a BIM model. Option A sees the model as a true-to-scale representation of the asset, option B interprets the model distorted in the same manner as the underlying CRS, and option C is a combination of the former. We explore each option with a case study and visual clues. We show that, while Option A is the most prevalent interpretation in the literature, experts from the infrastructure field prefer Option C, whose underlying rationale is explained in detail. We find that introducing infrastructural concepts to BIM methods requires the systematic resolution of georeferencing. We propose a workflow for the correct handling of any BIM geometries for construction projects. Additionally, we provide a decision diagram to help project stakeholders determine when the distortions of a CRS can be knowingly neglected.

Keywords: building information modelling, georeferencing, coordinate reference system, geodetic distortions, geometry representation

*Corresponding author, ORCID: 0000-0003-0387-3440

**Principal corresponding author, ORCID: 0000-0003-2088-7254

Email addresses: stefan.jaud@tum.de (Štefan Jaud), andreas.donaubauer@tum.de (Andreas Donaubauer), otto.heunecke@unibw.de (Otto Heunecke), andre.borrmann@tum.de (André Borrmann)

1. Introduction

1.1. Motivation

The architecture, engineering and construction (AEC) domain is experiencing a transition from two-dimensional (2D) planning to three-dimensional (3D) object-based modelling. Buildings and infrastructure assets are no longer described with drawings and accompanying documents; instead, they are represented by a digital model composed of parametric geometry representations in conjunction with a range of semantic information. The underlying concept of building information modelling (BIM) is steadily gaining importance supplanting conventional computer-aided design (CAD) practices and being implemented in every aspect of the very complex software and stakeholder landscape [16]. The methods and digital processes of BIM promise to entirely remove the need for physical documents altogether, with different actors exchanging digital models throughout the project. In order for this to work, these exchanges need to be clearly defined and the models must be interpreted indifferently and consistently by everyone involved [5].

Figure 1 shows an abstraction of the flow of data over the lifetime of a construction project [cf. 11]. The process chain starts with a survey of the construction site and its surroundings (whether an empty lot or an existing structure) and the production of an *as-is* model. The obtained geospatial data is usually stored, managed and merged with existing data from geographic information systems (GISs) during geospatial analysis. This data represents the initial state model (basis) for the AEC design processes. As the project proceeds, the models are iteratively evaluated, improved and exchanged between different actors, often using the non-proprietary Industry Foundation Classes (IFC) data format.

The *as-designed* model can then be returned directly to the geospatial analysis process, both to visualise the planned object in its geographical context and to test its impact and interaction with the environment (e.g. through noise or flooding simulations). As construction begins, the model needs to be realised in the material world and foundations at the construction site must be set out[1]. The progress of the construction is surveyed and *as-built* models are produced and joined with the *as-is* models during geospatial analysis. This cycle is repeated iteratively until completion of the project.

With the introduction of digital methods, an implicitly managed problem reappeared: the placement and true dimensions of the asset on the curved surface of the Earth. The selection and use of the project coordinate system (PCS) require close attention. *Georeferencing* refers to the process of specifying a geolocation (the placement of an asset on the surface of the Earth), as aptly described by Clemen and Görne [11]. In addition, it includes the definition of the parameters of the underlying coordinate system (CS), and thus the consequences of geodetic transformations (described in detail in Section 3.1).

If we are to change the established processes and design submissions, the problem of georeferencing needs to be adequately addressed [35].

[1] Also called a 'stake-out'.

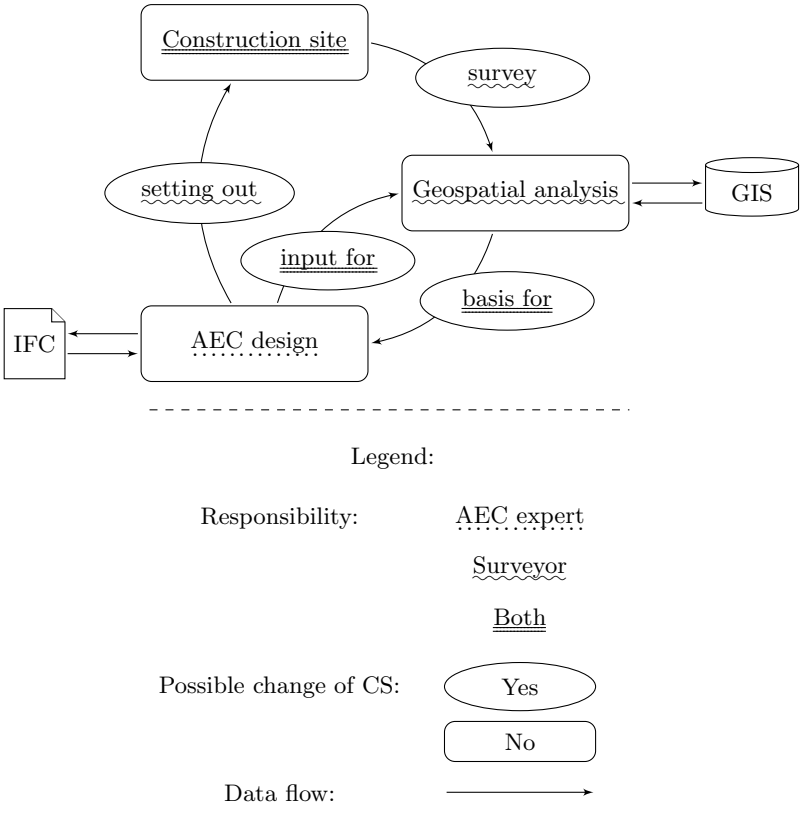

Figure 1: A conceptual data flowchart for the AEC industry. The digital model lies in a coordinate system that may be transformed during transitions between different stages.

1.2. Discrepancies

Digital engineering design is performed in the PCS, which is a Cartesian CS [48]. In this CS (X, Y, Z), the Earth's surface is modelled as an infinite, flat surface. All Z-planes of the PCS are equipotential surfaces[2] with any geographic elements, like mountains or trenches, deviating from the base height [34]. This corresponds to the intuitive human understanding of horizontality and of elevations on Earth, where it *seems* that the Earth is locally flat. In order to transform the curved surface of the Earth to a flat representation, some distortions are introduced through map projection.

All geospatial data comes in a well-defined compound coordinate reference system (CRS)[3]. We need to consider that projected CRSs possess a certain well-known discrepancy from the real world, which inherently includes a distortion in lengths, angles, and/or areas. For example, Mercator projection distorts lengths but preserves angles between any two points[4].

These distortions apply only along horizontal axes, are location-dependent and vary significantly in different CRSs. Since the map projection distorts lengths, the dimensions and position of objects as well as their shape are subject to discrepancies. They need to be accounted for when setting out the construction site. The scale factor m between a geospatial distance and its real-world dimension is defined as

$$m \overset{def}{=} \frac{\text{geospatial}}{\text{real world}} = 1 + 10^{-6}\Delta \ , \tag{1}$$

and is often conveyed as the difference factor Δ in parts-per-million (ppm). A scale in which $m < 1$ or $\Delta < 0$ means that the model is smaller than its real-world counterpart, while $m > 1$ or $\Delta > 0$ indicate the opposite.

This discrepancy has conventionally been handled by surveying engineers (Figure 1), and the problem itself was at least partly hidden from other stakeholders in the project, such as design engineers. However, with the introduction of BIM methods, it needs to be addressed appropriately, especially when large, linear objects are being modelled. There, the aspects of CRS and the distortions they imply have a much more significant impact on dimensions than when considering buildings with comparatively limited extents [10, 48].

1.3. Problem Definition

As BIM practices mature, the benefits they provide are spurring increased interest in the infrastructure sector [7, 13]. Additionally, as prefabrication directly from BIM models is gaining popularity, neglecting the scale factor can become a serious issue [e.g. 31, 51]. The discrepancies between the real world and the (projected) geospatial data may easily reach up to a few cm at a distance of 100 m, as explained in detail in Section 3.1.5 [20]. Projects that fail to account

[2] *Equipotential* surfaces are surfaces where any fluid without viscosity would not flow.

[3] The phrase *coordinate reference system* is an established term that refers to a *geodetic* coordinate reference system [24], as conveyed by the word *reference*.

[4] This is explained in more detail in Section 3.1.5. Since Mercator projections are used extensively in the AEC domain, this paper focuses only on these projections.

for this reality may operate under false interpretations and incur delays and increased costs.

This is why a clear understanding of the PCS specification used in the BIM model is needed. The main issue is the correct application of CRS to BIM data, or a lack thereof. This applies to models of building or infrastructure assets which are in either open formats (like IFC) or proprietary formats from software vendors. This paper explores the correct understanding and consideration of the scale factor from Equation (1) in the context of BIM.

The contributions of this paper are as follows:

1. It aims to serve as a knowledge bridge between AEC and geodetic experts, and between the BIM and geospatial worlds through the field of georeferencing. We achieve this by explaining the concepts from both fields, which may be familiar to experts in one but not the other.

2. We present three possible interpretations of geometries and locations within a BIM model as being a A) true or B) distorted representation of the asset or C) a combination of the two. We provide the reasoning behind these interpretations and evaluate their applicability to BIM models. They are discussed and depicted with practical examples to facilitate a better understanding of the problem. The goal is to familiarise the community with the subject and avert future mistakes [e.g. 12].

3. We provide a thorough analysis of all three options mentioned above and the rationale behind the most prominent proposed solution. We present a process map that can guide users to the correct geospatial interpretation of the contents of a BIM model. It can help software vendors implement correct algorithms and also enable project stakeholders to circumvent any problems derived from false understandings.

1.4. Structure of the Paper

We start the paper with an introduction, where we frame the problem, present our motivations and declare the objectives of this paper. Related works dealing with georeferencing of BIM models are presented in Section 2.

An in-depth explanation of geodetic as well as BIM models is given in Section 3. We present the well-known problems of mapping the curved surface of the Earth to a Cartesian CS, and vice versa in Section 3.1. If the reader's background is in geodesy, these topics are likely redundant. The BIM philosophy is described in Section 3.2, where the different geometric representations and positioning possibilities are highlighted. Readers from the AEC field are likely to already be familiar with these topics.

Section 4 describes the main contribution of this paper: the three interpretations of a BIM model, each illustrated with a case study. We evaluate these options with an extensive discussion in Section 5. We present the cost of ignorance of georeferencing in Section 5.2 and formulate recommendations for correct usage of georeferenced data in Section 5.3. We conclude this paper in Section 6 and offer a look forward.

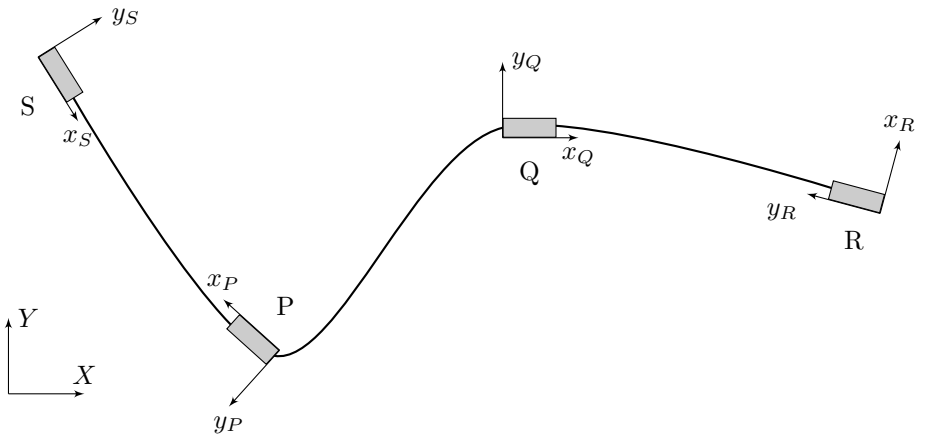

Figure 2: A hypothetical railway line with stations in cities S, P, Q, and R. Each station is a project on its own with its own $PCS_i = (x_i, y_i, Z), \forall i \in \{S, P, Q, R\}$. The railway track itself is planned in the global CS, thus $PCS_{\text{rail}} = (X, Y, Z)$. All CSs are right-handed [author redrawn from 10].

2. Related work

With the introduction of long objects from the infrastructure sector into the BIM context, georeferencing has become a topic of interest within the buildingSMART International (bSI) community [9]. Its members have addressed this issue in a recent publication called *Model Setup IDM* [10]. As the name suggests, the focus of the report was the model set-up process at the beginning of a BIM design project. The main goal of the report was to enable clear and concise model coordination for the duration of a project, which allows for meaningful clash detection. This is especially complex when many construction sites are included in a larger project [10].

They set up a hypothetical railway project as an example, in which they designed a new track with four stations (Figure 2). Each component was handled separately because they were managed by different design companies, so five models were passed to the coordinator: one for the railway line and one for each of the stations. The authors of the study considered the PCS used for the railway and each station, and demonstrated how to correctly define them and the relationships among them [10].

Their proposed solution was to use the established entities in the IFC data format to denote the underlying CRS. For transformations between different PCSs, they used 2D-Helmert transformations[5]. Additionally, they provided a guideline for the software implementers of the IFC schema for a currently widespread version, IFC2x3, and the latest official release, IFC4 [23]. Although the report provided a deep analysis of the geodetic background, it did not state whether or not a BIM model should be considered distorted or not.

Wunderlich and Blankenbach [50] denoted in their publication that a BIM model

[5]The Helmert transformation is thoroughly explained in Section 3.1.2.

is a true representation of the structure on site and should thus be considered not distorted. The importance of CRSs for the success of a BIM project was noted by Kaden and Clemen [27]. The authors expressed a recognition that "*their correct understanding is crucial especially in the infrastructure sector*" [27], but that "*most CAD data is created without this consideration*" [27]. They walked through an example study where they linked the CRS and the CS of the BIM model through an additional, intermediate CRS. This idea of using a local surveying CS, which represents the PCS, was presented by bSI as well [10].

In their latest study Clemen and Görne [11] looked at the different options provided by the IFC schema to specify the position of the model on Earth. They defined five Levels of GeoReferencing (LoGeoRef) and asserted that only the highest level provides enough information for precise surveying work. However, they made no mention of the *definition* of a PCS in terms of a CRS, describing only how the geolocation of the BIM model can be modelled within the IFC schema, and thus stored in IFC files.

A pair of recent studies from Uggla and Horemuz [48, 49] argued that a BIM model should be viewed as a "*1:1 representation . . . at the construction site*" [49]. In their view, IFC data is not georeferenced, per se, and must be transformed to georeferenced data accordingly. They considered the horizontal plane of the PCS in the BIM model to be tangent to the Earth at point of origin (POO), and thus it deviates from Earth's curved surface as it moves farther away from the POO. As such, the PCS's agreement with the real world stays within given tolerances only within a small area around the POO[6].

In order to transform the coordinates from the PCS to a CRS of choice, Uggla and Horemuz [48] proposed three options. The first option is drawn from Liebich et al. [32] and Borrmann et al. [4], and the other two are their own developments. They calculated the disagreements between the real world and the models for each of the three options and provided visual representations. However, no clear instructions or decision-making tools were provided for choosing the best option for future use. They concluded that "*the current implementation in the IFC schema is suitable for infrastructure design in areas where sufficiently accurate well-known map projections are available, and which are not too high above the reference ellipsoid*" [49]. They called for support of "*object specific map projections*" [49] and "*separate scale factors for different axes*" [49].

Ohori et al. [39] considered integrating BIM and GIS geometry by looking at the most prominent open standard formats from each world: IFC and CityGML, respectively. They demonstrated a best practice approach on several example buildings from the Netherlands. They paid close attention to correct geolocation, but they did not consider any geodetic distortions while converting the geometries. Liu et al. [33] provided a good overview of the state of the art of BIM and GIS integration. We disagree with their assertion that *The major difference between GIS and other information systems is that the GIS data are geo-referenced* [33] as shown within this study.

In our previous work, we have critically evaluated the current official IFC4

[6] In geodesy, this is called a 'topocentric system'. It is explained in detail in Section 3.1.2.

schema and its capability to store geospatial metadata [34]. With the introduction of BIM systems and the exchange of digital models this metadata must be handled as part of the process and correctly incorporated into the models. We found that the IFC4 version provides sufficient support for the typical case occurring in the majority of projects. However, based on two recent real-world infrastructure projects, the current schema is rendered as insufficient. We proposed two new IFC entities which would provide support for grid-shift parameter data-sets [34].

In another study, we looked at the Brenner Base Tunnel project in detail, in cooperation with the project team [35, 26]. The project-specific CRS was designed to minimize geodetic distortions, with the CRS and the PCS seen as identical. However, the PCS was defined in a way that accentuated the need for an expansion of the IFC schema. Even the simple inclusion of well-known text (WKT) strings would provide the needed flexibility to support even such peculiarities [25]. The proposal was tested on the custom CRS of the Brenner Base Tunnel, with positive results [26].

None of the studies above considered the research questions addressed in this paper; instead, each followed a single interpretation. We have only identified two studies which acknowledge the problem of different interpretations of BIM models.

Brenner et al. [8] produced guidelines for bridge design which included both distorted and undistorted interpretations of the BIM model. They published a process map that defined the points of transformations from distorted to undistorted modelling when exchanging information between different trades like road and bridge design. Their findings have been incorporated into this study in Section 5.2.3.

In one of our previous studies, Heunecke [20] considered the question of the interpretation of the PCS of BIM models. He presented the three possible interpretations discussed within this paper in Section 4. It was not his goal to propose one of these as the final solution.

An overview of the discussed literature and some additional studies is provided in Table 1, where BIM model interpretation is marked according to our understanding of each paper.

3. Theoretical Background

3.1. Geodesy

The geospatial data used in a design process is saved in a well-defined CRS, which is composed of two independent systems: the location and the height reference. The former is composed of the geodetic datum and a map projection (which flattens the curvature of the Earth's) and the latter is based on a vertical datum. Together, this is a compound CRS [24]. It is important to fully understand these models if we are to answer the research questions at hand. To this end, the following subsections provide a detailed overview, and the rationale behind, the geodetic models relevant to this study. More detailed explanations can be found in the ISO 19111:2019 [24] standard.

Table 1: An alphabetical overview of the related studies, with their interpretation of the spatial contents of BIM models marked with an 'X'. The column categories correspond to the three possible interpretations explored in detail in Section 4.

Interpretation	undistorted	distorted	combination
Borrmann et al. [4]		unclear	
Brenner et al. [8]			X
buildingSMART International [10]		unclear	
Clemen and Görne [11]	X		
Heunecke [20]	X	X	X
Jaud et al. [26]		X	
Kaden and Clemen [27]	X		
Liebich et al. [32]		unclear	
Markič et al. [34]		X	
Markič et al. [35]		X	
Ohori et al. [39]	X		
Uggla and Horemuz [48]	X		
Uggla and Horemuz [49]	X		
Wunderlich and Blankenbach [50]	X		
Option (see also Section 4)	Option A	Option B	Option C

3.1.1. Model of Earth

In a global sense, a Cartesian CS (X, Y, Z) can be anchored to the Earth's centre of mass. This is an Earth-centred, Earth-fixed (ECEF) CRS in geodesy and is defined as follows (Figure 3) [10]:

- The Z-axis spans from the geocentre through the international reference pole (IRP) and coincides with the Earth's rotational axis.
- The X-axis is the intersection of the international reference meridian (IRM) and the mean equatorial plane (MEP).
- The Y-axis is then defined so that it spans a right-handed orthogonal CS.

The unit of measurement (UoM) is metres on all axes. This model is extensively used in satellite-based positioning. However, such a model is not really useful in the AEC industry, since it does not provide support for an intuitive understanding of *horizontality*, as described in Section 1.2. When AEC experts discuss about the form of the Earth, they implicitly refer to the form of the equipotential gravity field. Here, geographical elements like mountains and trenches deviate from the base height[7], $H = 0$.

Figure 4 depicts a mathematical and physical model of the Earth. Since the Earth is basically a sphere that is squashed at the poles due to centrifugal forces, a very strong mathematical approximation is a rotational ellipsoid[8], which is an ellipse rotated around its minor axis (Figure 4a) [24]. In a geodetic context, it is

[7]This base height is often set to mean sea level. However, a CRS can define other reference surface(s) if this brings enough benefits to justify the deviation from the convention [35].

[8]An excellent explanation of the error between an ellipsoid and a sphere can be found through StackExchange [45].

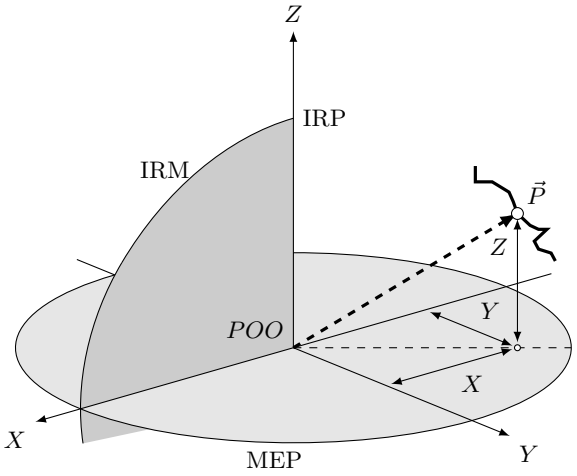

Figure 3: ECEF CRS with the POO defined as Earth's center of mass, IRP defining the Z axis, MEP defining the (X, Y) plane, and IRM defining the X axis. The point $\vec{P}$ is uniquely defined by its three coordinates (X, Y, Z) [author redrawn from 10].

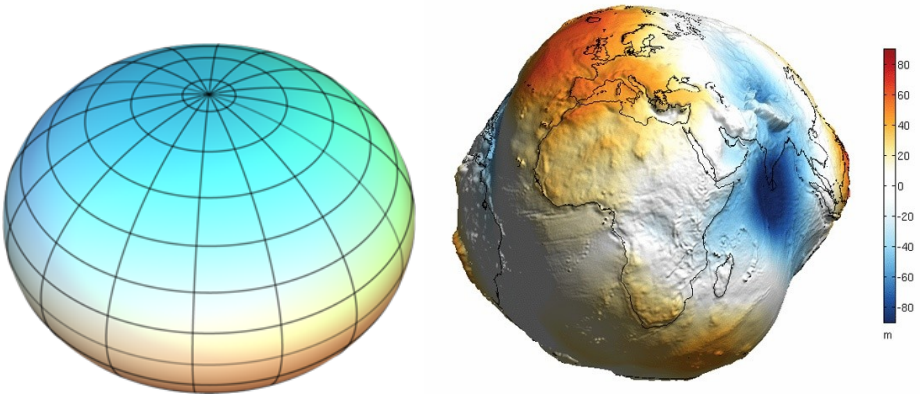

(a) (b)

Figure 4: Images of the models of the Earth: the mathematical model (a) is a rotational ellipsoid [14], and the physical model (b) is a geoid or "potato" [21]. The surfaces represent base surface, $h = 0$, and the equipotential surface, $H = 0$, respectively. The differences on the geoid are exaggerated and shown relative to the ellipsoid WGS84.

common to define additional variables to simplify the calculations as presented in Table 2 [17, 29]. This table also includes exemplary values for widely used ellipsoids from the World Geodetic System 1984 (WGS84) and the Geodetic Reference System 1980 (GRS80) [17].

Gravimetric measurements can determine the natural equilibrium form of the Earth – the so-called geoid. This physical model of the equipotential surface of Earth is often dubbed 'the potato' (see Figure 4b). These two forms define separate reference surfaces for measuring elevation. The height of a specific point above the ellipsoid is called the ellipsoidal height, h, which must be strictly distinguished from the physical height, H, which is relative to the geoid. The

Table 2: The parameters of a rotational ellipsoid and their interdependency with exemplary values for the WGS84 and GRS80 ellipsoids. The ellipsoid is described by two independent parameters, normally the major axis, a, and the inverse flattening, f^{-1}, in the geodetic context [17, 24, 29].

Variable	Parameter	Equation	WGS84	GRS80
a	major axis	$a = b/(1-f)$	6 378 137.0 m	6 378 137.0 m
b	minor axis	$b = a(1-f)$	6 356 752.314 245 m	6 356 752.314 140 m
e	eccentricity	$e = \sqrt{a^2-b^2}/a$	0.081 819 191	0.081 819 191
e'	second eccentricity	$e' = \sqrt{a^2-b^2}/b$	0.082 094 438	0.082 094 438
f	flattening	$f = (a-b)/a$	1/298.257 223 563	1/298.257 222 101
n	third flattening	$n = (a-b)/(a+b)$	0.001 679 220	0.001 679 220

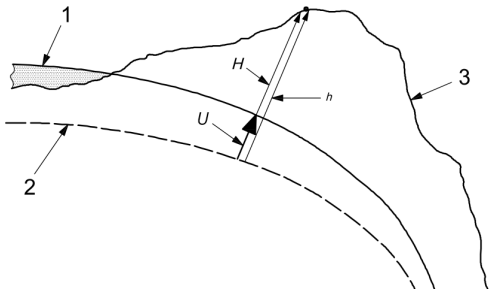

Figure 5: The ellipsoid (2) and geoid (1) heights of Earth (3) are h and U (denoted N in the literature), respectively. H is the gravity-related height measured along the direction of gravity [24, 47].

differences between them are called *undulations*, U[9] (see Figure 5), which are defined as

$$h = H + N \stackrel{def}{=} H + U\,, \tag{2}$$

and can amount to up to $U = \pm 100$ m from the WGS84 ellipsoid (Figure 4b). At this point, a strict distinction must be made between the geoid (with orthometric heights) and the quasi-geoid (with normal heights). This results from the way the equilibrium figure is calculated and will not be discussed here [see 47, for more details].

3.1.2. Topocentric System

The simplest example of a CRS on Earth's surface is a topocentric system. A local Cartesian CS (x, y, z) is defined at a chosen POO on the Earth's surface (hence the prefix *topo*). The z-axis coincides with the negative direction of the gravity pull at the POO, while the x and y axes are chosen to form a Cartesian CS in the plane perpendicular to that z-axis. Note that such a topocentric CRS is defined as a left-handed system in surveying and as a right-handed system in the AEC domain.

[9] Undulation is usually given the symbol N in the literature [24]. We have decided to use U in this paper in order to differentiate it from the Northing coordinate, N.

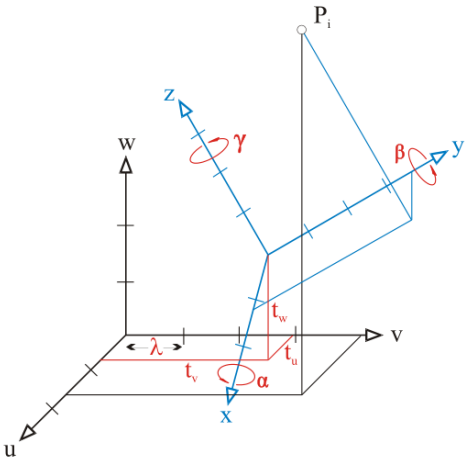

Figure 6: 7-parameter Helmert transformation from Equation (3). The originating coordinate system is (x, y, z), the transformed is (u, v, w). The 7 parameters $(t_u, t_v, t_w, \lambda, \alpha, \beta, \gamma)$ are also shown.

In order to transform the coordinates between two right-handed Cartesian CSs (for example from ECEF to a topocentric system – though this is not done in practice), a relationship between the originating (x, y, z) and transformed coordinates (u, v, w) needs to be established [48]. A so-called 7-parameter Helmert transformation for point $P_i = [u_i, v_i, w_i]^T = f([x_i, y_i, z_i]^T)$ is defined as (Figure 6)

$$\begin{bmatrix} u_i \\ v_i \\ w_i \end{bmatrix} = \begin{bmatrix} t_u \\ t_v \\ t_w \end{bmatrix} + \lambda R(\alpha, \beta, \gamma) \begin{bmatrix} x_i \\ y_i \\ z_i \end{bmatrix} , \tag{3}$$

where

$$R(\alpha, \beta, \gamma) = \begin{bmatrix} c\gamma\ c\beta & c\gamma\ s\beta\ s\alpha + s\gamma\ c\alpha & -c\gamma\ s\beta\ c\alpha + s\gamma\ s\alpha \\ -s\gamma\ c\beta & -s\gamma\ s\beta\ s\alpha + c\gamma\ c\alpha & s\gamma\ s\beta\ c\alpha + c\gamma\ s\alpha \\ s\beta & -c\beta\ s\alpha & c\beta\ c\alpha \end{bmatrix} , \tag{4}$$

with c and s standing for *cos* and *sin* functions, respectively.

As noted by Uggla and Horemuz [48], a topocentric CRS only represents the equipotential surface of Earth well in close proximity to the POO. The horizontal plane of the CS deviates increasingly from the curved surface of Earth with increasing distance from POO. As such, following the curved Earth during construction while interpreting the model as is (i.e. flat) induces a steadily growing error as we move farther away from the POO. For this reason, this CRS is only useful for small construction sites where these discrepancies remain negligible. For projects with a greater extent, a CS needs to be defined which allows for clear transformations while still retaining the human understanding of horizontality as described in Section 1.2. The exact values distinguishing small and big extents are discussed in Section 5.2.3.

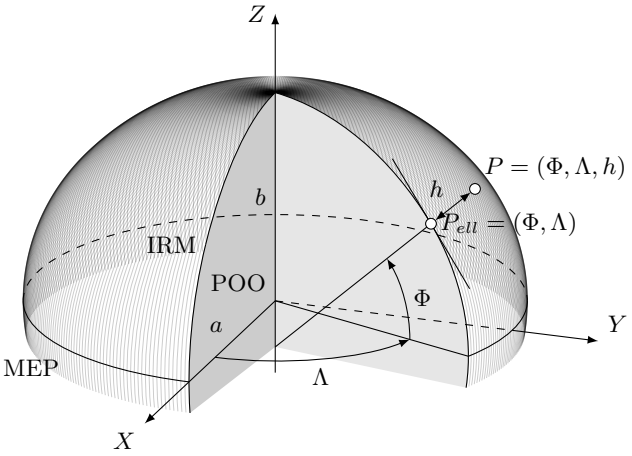

Figure 7: Latitude and longitude (Φ, Λ) uniquely define a point, P_{ell}, on an ellipsoid with major and minor axes a and b, respectively (only the top half is shown). Together with the ellipsoidal height, h, measured perpendicular to the ellipsoid surface, any point P can be referenced by its three coordinates as $P = (\Phi, \Lambda, h)$ (cf. Figure 3).

3.1.3. Geodetic Datum

As shown above, an ellipsoid is a good mathematical approximation of the shape of Earth. A geodetic datum relates a specific ellipsoid to the Earth by providing its form, position and orientation in space. The use of spherical coordinates offers a way of referencing points on ellipsoidal and thus Earth's surface as shown on Figure 7. The latitude, Φ, and longitude, Λ, denote the angles from the reference lines (IRM and MEP, respectively). A pair of angles (Φ, Λ) defines a unique location on the ellipsoid.

Throughout history, many ellipsoids have been defined and used with different areas of best fit. The *best fit* objective is to minimise the differences between the geoid and the ellipsoid in a specific area or in a global context. In the case of a *local* geodetic datum, the coordinates of reference points on Earth are defined to be identical with the coordinates on the ellipsoid, and the Earth's surface normals (plumb lines) should coincide as closely as possible with the surface normals on the ellipsoid at these reference points. In the case of a *global* geodetic datum, the centre of the ellipsoid is set to be identical with the Earth's centre of gravity and its minor rotational axis coincides with the Earth's mean rotational axis (through the IRP). The European Terrestrial Reference System (ETRS) is a three-dimensional (x, y, z) geodetic reference system, which is affixed to the Eurasian continental plate and was identical to the International Terrestrial Reference System (ITRS) in 1989. While the coordinates of the ITRS have had to be redefined repeatedly, especially due to global plate tectonics, the coordinates of the ETRS used in Europe are largely time-constant. For the specification of ellipsoidal coordinates, the parameters of the GRS80 are used within the ETRS.

3.1.4. Vertical Datum

There are several possible definitions of elevation on Earth. One of them is to define verticality on Earth's surface as parallel with direction of Earth's gravity

pull, so that the vertical axis, H, follows the plumb line. In this way, water does not flow between two points with the same elevation, and this corresponds with the human notion of elevation and is very practical in construction. For easier notation, the coordinate value is usually given as a distance to some reference surface and not to the POO [24]. This reference surface is one of Earth's gravity field equipotentials and is set as the zero orthogonal height, $H = 0$. The surface most commonly chosen is mean sea level [17]. An example of a vertical datum is the Deutsches Haupthoehennetz 2016 (DHHN 2016), used mainly in Germany.

Knowing a point's orthogonal height, H, and the undulation between the chosen geodetic and the vertical datum, U, any point can be uniquely referenced as

$$P = (\Phi, \Lambda, h) = (\Phi, \Lambda, H - U) \ . \tag{5}$$

This is reflected in Equation (2) and Figures 5 and 7.

3.1.5. Projected CS

The horizontal Cartesian plane (X, Y) of a PCS is obtained by projecting the curved ellipsoidal surface onto a plane using one of many types of map projection [44]. First, the ellipsoidal coordinates (Φ_i, Λ_i) get mapped to the geodetic coordinates. For example, with the widely used Universal Transverse Mercator (UTM) projection, these are Easting and Northing (E_i, N_i), which are used hereinafter. A comprehensive procedure is provided in Appendix A for both the transformation $(E_i, N_i) = f_{\text{proj}}(\Phi_i, \Lambda_i)$ and the reverse transformation $(\Phi_i, \Lambda_i) = f^{-1}_{\text{proj}}(E_i, N_i)$. The Cartesian coordinates (X_i, Y_i) at the construction site are then connected to geodetic coordinates using the 2D version of Equation (3) with $t_w = \alpha = \beta = 0$:

$$\begin{bmatrix} E_i \\ N_i \\ 0 \end{bmatrix} = \begin{bmatrix} E_{POO} \\ N_{POO} \\ 0 \end{bmatrix} + \lambda R(0, 0, \gamma) \begin{bmatrix} X_i \\ Y_i \\ 0 \end{bmatrix} \ , \tag{6}$$

where (E_{POO}, N_{POO}) represent the geodetic coordinates of the PCS's POO[10].

Projecting the curved surface of an ellipsoid onto a plane without any deformation is geometrically impossible [44]. Hence, a map projection can preserve only one of the following: angles, distances or surface areas. The compromise most frequently chosen in large-scale topographic applications or cadastral surveying is to preserve angles by using a conformal map projection. The two most commonly used map projections are the Gauss-Kruger (GK) and the UTM projections [34].

To keep the distance and surface area distortions within an acceptable range, strips of the ellipsoid are defined and projected onto a cylinder with an elliptical

[10]Many geodetic CSs are left-handed, inlcuding (N, E, H). Notice that Northing is the first coordinate. In this paper we knowingly neglect this fact in lieu of simplicity and consider all CSs to be right-handed, thus switching the order of the coordinates in Equations (3) and (6). This is also the basis for ISO 10303-42:2019 [22], upon which the IFC data format bases: *All geometry shall be defined in a right-handed rectangular Cartesian coordinate system with the same units on each axis.*

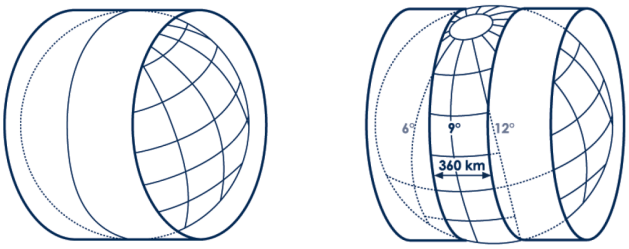

(a) (b)

Figure 8: Different ways of projecting an ellipsoid on a cylinder: (a) GK projection and (b) UTM projection [modified from 19].

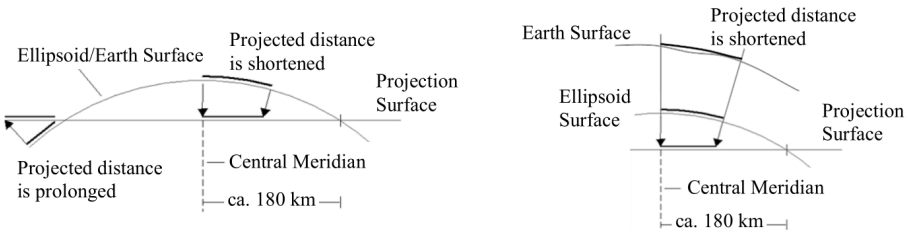

(a) (b)

Figure 9: The distortions induced by (a) the UTM projection and (b) height reduction [reproduced with permission from 27].

cross section (Figure 8). Note that the borders of the strips are defined by meridians on the ellipsoid; thus, the strips are tapering with increasing distance from MEP. This can be clearly seen on Figure 8b, where the distance between the intersections of the projection cylinder with the ellipsoid is constant, whereas the distance between the meridians on the ellipsoid gets shorter from the equator towards the poles.

The GK projection uses a cylinder that touches the ellipsoid at a meridian (Figure 8a). Therefore, only the distances along the meridian are not distorted ($\Delta_{0,\mathrm{GK}} = 0\,\mathrm{ppm}$) and the distortion increases for locations farther away from the meridian. This is why the strips of the projection have a width of 3°, where the maximum scale is $\Delta_{\mathrm{border,GK}} \approx 150\,\mathrm{ppm}$ [24, 27].

In the UTM projection, the cylinder intersects with the ellipsoid approximately 180 km east and west of the central meridian of a specific zone, which has a width of 6° (Figure 8b). Thus, the central meridian is shortened with $\Delta_{0,\mathrm{UTM}} = -400\,\mathrm{ppm}$ and the borders lengthened for $\Delta_{\mathrm{border,UTM}} \approx 160\,\mathrm{ppm}$. This keeps the distortions in an acceptable range, even at the borders of the zone [24, 27].

A cross section of the UTM projection cylinder and the ellipsoid can be seen in Figure 9 [27]. All geospatial data lie on the chosen ellipsoid and must first be projected there from their elevations. This process causes additional distortion in the distances as shown in Figure 9. The factors of these distortions are explained thoroughly in Appendix A.

3.1.6. Compound coordinate reference system

In summary, a CRS defines the underlying CS of all geospatial data and is composed of multiple parts. The choice of ellipsoid's size, position and orientation with regard to the Earth together with the elevation reference define the geodetic and vertical datums, respectively. The chosen map projection defines the method by which the double-curved surface of the ellipsoid is mapped to the Cartesian CS.

The map projection, together with the geodetic datum, is called a *projected* CRS. When combined with a vertical CRS, the reference system is called a *compound* CRS [24]. The European Petroleum Survey Group (EPSG) database contains a comprehensive collection of these references, systems, and their combinations; nearly 6000 CRSs from around the world are currently listed together with datum definitions and transformations [17].

The distortions ($[\mathrm{cm}/100\,\mathrm{m}] = 100\,\mathrm{ppm}$) induced by the chosen ellipsoid, map projection, and height above the projection surface are illustrated in Figure 10 for the state of Bavaria, Germany [15]. Figure 10a shows the distortions induced by the UTM map projection from the ETRS geodetic datum. The UTM zone 32 (UTM32) has its central meridian at 9° E, which goes through the western tip of Bavaria. The scale there is therefore $\Delta_{\mathrm{UTM32;9}} = -4\,\mathrm{cm}/100\,\mathrm{m}$. Although the UTM32 stops at 12° E (where zone 33 begins), the scale is still at a manageable $\Delta_{\mathrm{UTM32;12}} = 1.6\,\mathrm{cm}/100\,\mathrm{m}$, so the Bavarian state decided to extend zone 32 for reasons of simplicity. This way, all Bavarian geospatial data is within the same zone and complicated calculations at the zone change can be omitted. However, this means that the distortions at the far eastern edge of Bavaria reach a non-negligible $\Delta_{\mathrm{UTM32;13.8}} = 11.7\,\mathrm{cm}/100\,\mathrm{m}$, which corresponds to $m_{\mathrm{UTM32;13.8}} = 1.00117$.

Figure 10b shows the distortions due to the vertical distance from the projection surface as seen on Figure 9, right. Here, the distortions induced by using the ETRS geodetic datum with the underlying ellipsoid GRS80 and the DHHN 2016 vertical datum is shown.

To determine the scaling factor induced by all of these concepts at a given point, the distortions caused by projection m_{proj} and height reduction m_h from Equations (A.5) and (A.14) need to be multiplied together (provided in Appendix A)

$$m_{CRS}(\Phi, \Lambda, h) = m_{proj}(\Phi, \Lambda) \cdot m_h(\Phi, h)\,, \tag{7}$$

where h is defined in Equation (2). This scale function only applies to the horizontal axes (E and N) and does not influence the vertical values, despite being dependant on both the location and elevation values. Note that m_{CRS} is a function of location as well as the chosen CRS, and it can be set to an approximated constant value only within a limited range.

3.2. Building Information Modelling

BIM stems from CAD methods, where 3D object-oriented modelling has found its use in parametric design and semantically rich data. Instead of drawing lines with multiple geometric constraints on different layers that convey semantics, objects are contained in a BIM model which inherently provides all kinds of

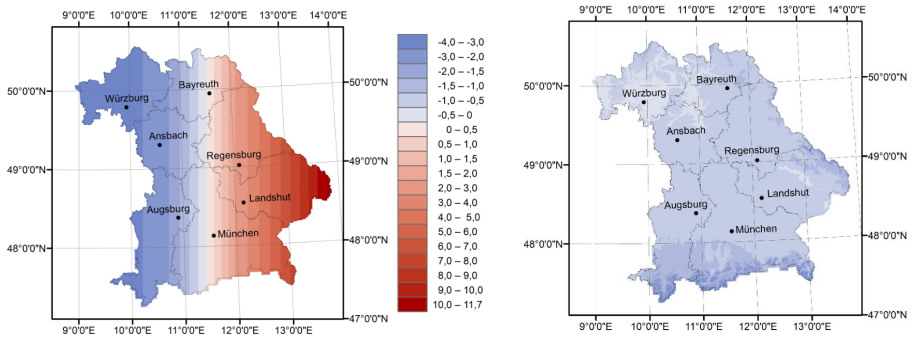

(a) (b)

Figure 10: The values of length distortions [cm/100 m] from Figure 9 shown using Bavaria, Germany, as an example. (a) Distortions due to the UTM projection from GRS80 ellipsoid (see also Figures 8b and 9a). Note: Per definition, there should have been a zone change at 12° from UTM32 to UTM33; however, Bavaria considered to have all its geospatial data in one zone. (b) Distortions due to height reduction $H \approx h \neq 0$ to GRS80 ellipsoid (see also Figures 5 and 9b) [15].

constraints and rich semantic data. Resources like drawings, bills of quantities, time tables and more can be automatically derived from a BIM model, and so only the model needs to be exchanged between stakeholders. Additionally, BIM models support other use cases, such as clash detection, automatic prefabrication and construction simulation. Potential errors identified can thus be averted even before construction has started.

One of the foundations of BIM is the parametric 3D modelling of objects that is supported by the majority of software vendors. With the introduction of constructive solid geometry (CSG), complex geometries previously depicted on a blueprint could be implicitly described according to their construction steps. In the next subsections, we cover the principal concepts of 3D modelling in BIM: i) the positioning and CSs involved in placement, and ii) different geometry representations. Both concepts are influenced by the different interpretations of the underlying CS and are therefore important to understand in the scope of this research[11]. While there are many different placements and geometry representations available in software products, we focus in our paper on those present in the IFC standard [23].

3.2.1. Positioning

Each element's geometry resides within a local CS with a well-defined POO and orientation of the coordinate axes. This CS is usually a right-handed Cartesian CS (x, y, z), as this is intuitive and simple [22]. The coordinate axes scale with each other, by definition, and have the same UoM.

The position of this CS is specific to each object and is always defined relative

[11] Strictly speaking, all properties attached to an object containing values for lengths, areas, or volumes are influenced too, and should have been considered. However, we assume that the geometry and location are depicted with the corresponding representations, and we can therefore exclude these quantities from consideration.

to another CS. This can be the global CS of the model (*absolute placement*) or another local CS of an element higher in the hierarchical structure (*relative placement*). There are multiple possibilities for relative placement, which are described in the following paragraphs. These options can be combined freely and used recursively, *ad libitum*. To simplify the notation, we use (x, y, z) for the originating CS and (u, v, w) for the object's CS.

Local Placement. The definition of a CS using local placement is common practice in building design. This is done using Equation (3) with $\lambda = 1$ (Figure 6).

For example, a wall is placed within a building storey with a POO at (t_u, t_v, t_w). The u axis is defined to run along the wall's centreline, the w axis functions as the z axis of the storey ($\alpha = \beta = 0°$) and $v = w \times u$ such that it defines a right-handed Cartesian CS.

Grid Placement. Multiple elements can be placed in a grid-like constellation. The base point, the distance step(s) and the reference direction(s) uniquely define the POO of each element. The (u, v, w) axes are additionally defined once for all elements and may diverge from the reference directions (x, y, z).

A simple example is the raster-like representation of a digital terrain model (DTM). In this case, only the first point has its (x_0, y_0) coordinates and the steps d_x and d_y are given. The heights are represented with a 2D array of values in the parent's CS, $w_{i,j} = z_{i,j}$, where i and j represent the indices of the point $P_{i,j}$ in the array. The coordinates of the point are thus $P_{i,j} = (u, v, w)_{i,j} = (x_0 + id_x, y_0 + jd_y, z_{i,j})$.

Linear Placement. Another possibility is to define the CS of an element relative to a curve. This so-called 'linear placement' is common practice in infrastructure design. The POO is placed in a point, which is placed a certain distance along the basis curve (directrix).

For the definition of the coordinate axis, there are two possibilities which are differentiated during the definition of the w axis.

I) The u axis follows the tangent of the curve at the POO in the direction of increasing distance from the beginning of the curve. The v axis is then defined to lie on the (x, y) plane to the left of the curve, with the w axis being the cross product of the two: $w = u \times v$. This yields a right-handed Cartesian CS.

II) A slightly different possibility is to keep the direction of the w axis the same as the z axis. The u axis is then defined as the projected tangent direction of the curve at the POO on the (x, y) plane and the v axis is the cross product of the other two: $v = w \times u$. This again yields a right-handed Cartesian CS.

An example of the first option is the placement of cross sections in a tunnel dug with a tunnel boring machine (TBM). Here, the plane of the front of TBM, and thus the scans and profiles, always lies perpendicular to the base curve of the tunnel. An example of the second option is the placement of a typical supporting column on the railing of a staircase. It is placed parallel to the staircase's main directrix, but the vertical direction remains that of the risers.

3.2.2. Geometry

There are multiple possible representations of 3D geometry in a BIM model [43]. These can be split in two categories: implicit and explicit representations. The former are *top-down* representations, where the geometry is described with the required steps and parameters from its design process. For example, a cube can be uniquely described by its centre point, its side length, and the orientation of two of its axes in space. The latter representations take a *bottom-up* approach to building the geometry, with 3D vertices that are connected to higher-dimension geometries like edges, surfaces, and, eventually, solids. Again, a cube can be described by its 8 vertices in space, the 12 sides connecting them, and the 6 surfaces bounded by these elements, which enclose and complete the cube.

In the following subsections, we depict individual geometries with an exemplary geometry: a frustum of a right circular cone. Such a geometry is often used at bridge approaches for embankments if the abutment was not designed with retaining walls. Figures 11 and 12 show its explicit and implicit representations, respectively.

Boundary representation. An efficient and flexible explicit geometry representation is the boundary representation (BRep) depicted in Figure 11a. Here, 3D vertices (represented by points) make up the basis for higher-dimension geometries. These are linked to form (potentially curved) edges, such as non-uniform rational B-splines (NURBS), arcs, or simple polylines. Solids are bordered by (potentially curved) faces bounded by the lines.

The example in Figure 11a was built up from eight vertices. These are connected by nine edges: seven lines and two B-splines, which approximate a circular arc. Each arc is defined by three vertices as described by Abedallah [1]. In turn, the edges border five faces, which enclose the volume.

Tessellated Geometry. The tessellated representation is a special type of BRep that strives for simplicity. It consists of an array of 3D points connected in loops; hence the name 'tessellated'. The loops represent polygonal planar surfaces, most commonly triangles. In order to achieve its simplicity, tessellated geometries make a trade-off between precision and data required to encode them. This is clear for curved geometries, which could theoretically be split into an infinite number of polygons.

The example in Figure 11b consists of ten points. The B-splines from Figure 11a have been approximated by four points and the curved surface by three trapezoids. The figure also shows the tessellation that would be used if the only shape allowed for a face were a triangle, as is the case in some 3D systems. This could be refined infinitely if higher precision is needed, but the amount of data grows as well. Each new point that is added improves the approximation of the arc, but it adds an additional trapezoid (or pair of triangles) to the slope, for a total of four additional triangles that must be defined and stored in memory (1 top, 1 bottom and 2 on the slope).

Sweep. A swept geometry is an implicit geometric representation that is based upon a shape (cross section) that is extrapolated (extruded) along a basis curve (directrix). This implicit representation is often used in infrastructure, e.g. a rail profile that is swept along the railway's alignment. If the cross section

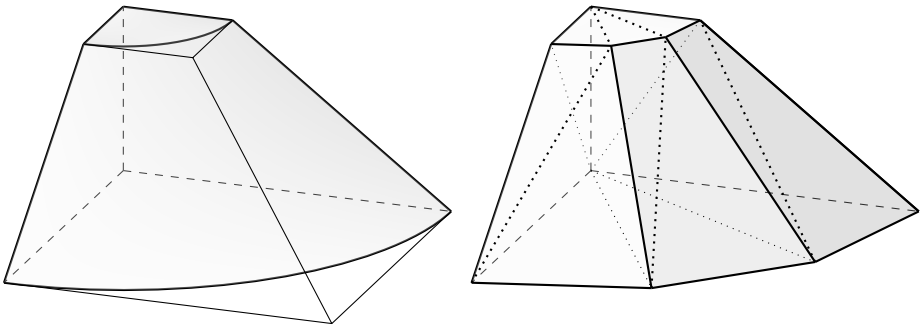

(a) (b)

Figure 11: Example of explicit geometry representations in BIM models: a frustum of a right circular cone. (a) A boundary representation. The front face is a NURBS surface bordered by two lines and two B-splines. (b) Tessellated geometry. Dotted lines show how the faces would be defined when only triangles must be used.

never changes along the line, the operation is called *sweeping*; otherwise it is *lofting*. If the basis curve is a straight linear segment, the operation is called *extrusion*. The cross section may be a single line, a NURBS or a closed curve that is empty or full. The results of extruding these cross sections would be the creation of a plane, a curved surface, a hollow pipe-like object and a solid body like a cylinder, respectively.

The example in Figure 12a shows a vertical full profile being extruded along a quarter-circle directrix. The profile has a trapezoidal form, which could have been defined by four points or lofted from the bottom to the top line in the vertical direction. The path itself can take many forms; in this case it is an arc, defined by its centre on the vertical line of the profile, with the radius being the width of the trapezoid at that height.

Constructive solid geometry. Constructive solid geometry (CSG) representation uses the principles of point set theory to define elementary building blocks and join them using Boolean operators. In this way, the geometry is described by the operations that must be applied to construct it. The base blocks may be simple geometric bodies, like cubes or spheres defined by their parameters or geometries of other geometric representations. The possible Boolean operators are union ($A \cup B$), intersection ($A \cap B$) and subtraction ($A - B$).

Figure 12b shows the example geometry with two base forms used to produce it. The right cone and the cuboid are positioned relative to one another in such way that the cone's centre and cuboid's side coincide. The desired geometry is achieved by intersecting these two primitives.

4. Spatial Interpretation of BIM Models

This section handles the main question as posed in Section 1.3. With the background knowledge provided in Section 3, it can be reformulated as follows: *What is the functional connection between the project scale, m_p, of a BIM model and*

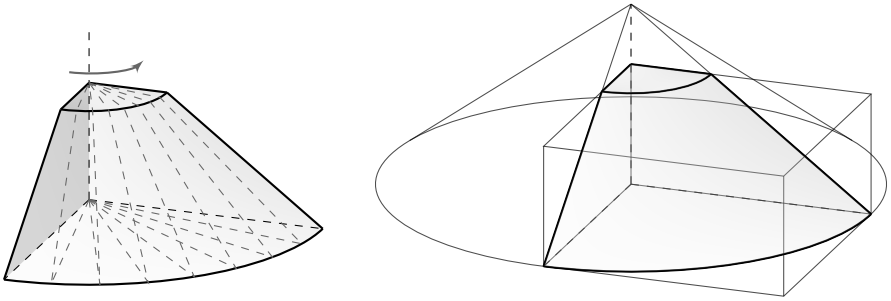

(a) (b)

Figure 12: Examples of implicit geometry representations in BIM models: a frustum of a right circular cone. (a) Sweep of the trapezoid along a quarter-circle directrix defines the frustum. (b) Constructive solid geometry (CSG): the primitives cuboid and right circular cone intersect to produce the frustum.

the scale of the underlying geospatial data, m_{CRS}? That is, how to properly define this function, which is a variable locus function:

$$m_p \stackrel{def}{=} f(m_{\text{CRS}}) \ . \tag{8}$$

Since the value of m_{CRS} varies continuously from point to point, complex distortions are not uncommon (e.g. straight lines can become curved lines in another CRS).

We stress again that this spatial interpretation only applies to the horizontal, and not the vertical, extent of the BIM model (Equations (7) and (8)). Whereas m_{CRS} is mostly dependant on longitude, elevation, lastly latitude (Equation (7)), m_p can be set to a constant value with certain assumptions (discussed in detail in Section 5). This text uses the words '*factor*' and '*function*' interchangeably for m_p.

Additionally, m_p is not the same as the scale factor of a drawing, instead it indicates the distortion of lengths between the model and on-site representation due to the underlying CRS features.

In the following subsections we present the three options of defining the function in Equation (8) as well as a case study for each option to better depict their approach to the interpretation of a BIM model.

4.1. Options

We have identified three interpretations of the spatial extents of a BIM model (Figure 13).

Option A: We consider a BIM model to be a true representation of a real asset. With $m_p = 1 + 0m_{\text{CRS}}$, the dimensions and relative positioning of the objects in the model correspond to those in nature.

However, the underlying geospatial data used during the design process first needs to be transformed back to its true dimensions by using the inverse of its underlying CRS, i.e. by m_{CRS}^{-1} (Figure 13a). This means that the true nature

Table 3: An overview over the case studies presented in Section 4.2.

Section	Case study	Interpretation	Reference
4.2.1	*Embankment*	Option A	Section 3.2.2
4.2.2	*Road*	Option B	Equation (7)
4.2.3	*Railway*	Option C	Figure 2

of the curved Earth is represented in the model itself, and that the Z planes *no longer* correspond to equipotential surfaces. If this assumption is still held, agreement is only maintained in a small area around the POO [48].

Option B: We consider the models to be distorted by the scale function $m_p = m_{\mathrm{CRS}}$ grounded in the compound CRS of the underlying geospatial data used for design. This option is the opposite of Option A (Figure 13b).

When setting out the construction site, the model must be transformed back to true dimensions by m_{CRS}^{-1}. Knowing this, the design norms need to be adjusted before use, e.g. if a building edge must stand d_{norm} away from the street, the correct value used for the design is $d_{\mathrm{design}} = m_{\mathrm{CRS}}\, d_{\mathrm{norm}}$.

Option C: This option is a combination of Options A and B (Figure 13c). We consider the models for buildings and infrastructure objects separately, interpreting their spatial extents according to Option A and Option B, respectively. In this case, *buildings* are all structures with limited extents in horizontal dimensions (e.g. houses, skyscrapers and short bridges and tunnels), while *infrastructure objects* include all elongated objects (e.g. roads and railways).

4.2. Case Studies

To better visualise the differences and consequences of spatial reference, we provide three simple theoretical case studies, each establishing a different scenario (Table 3).

1) The first case study, *Embankment*, was introduced in Section 3.2.2. It provides an overview of the possible geometry representations and their influence on the computed volumes. This influence is shown in Section 4.2.1 in order to distinguish it to the influence of geodetic distortions on the volume depicted in Section 4.2.3.

2) The second case study, *Road*, is a long object with a simple geometric representation, where a rectangular cross section is swept along a predetermined route. It shows the difficulties of the location-dependent distortions of a CRS from Equation (7).

3) The third case study, *Railway*, considers the railway and its stations from Figure 2. Here, the different spatial references of the BIM objects, as well as the difficulties of their synchronisation, are highlighted.

4.2.1. Embankment

The embankment from Figures 11 and 12 is taken as our first case study, with which we highlight the different geometry representations listed in Section 3.2.2.

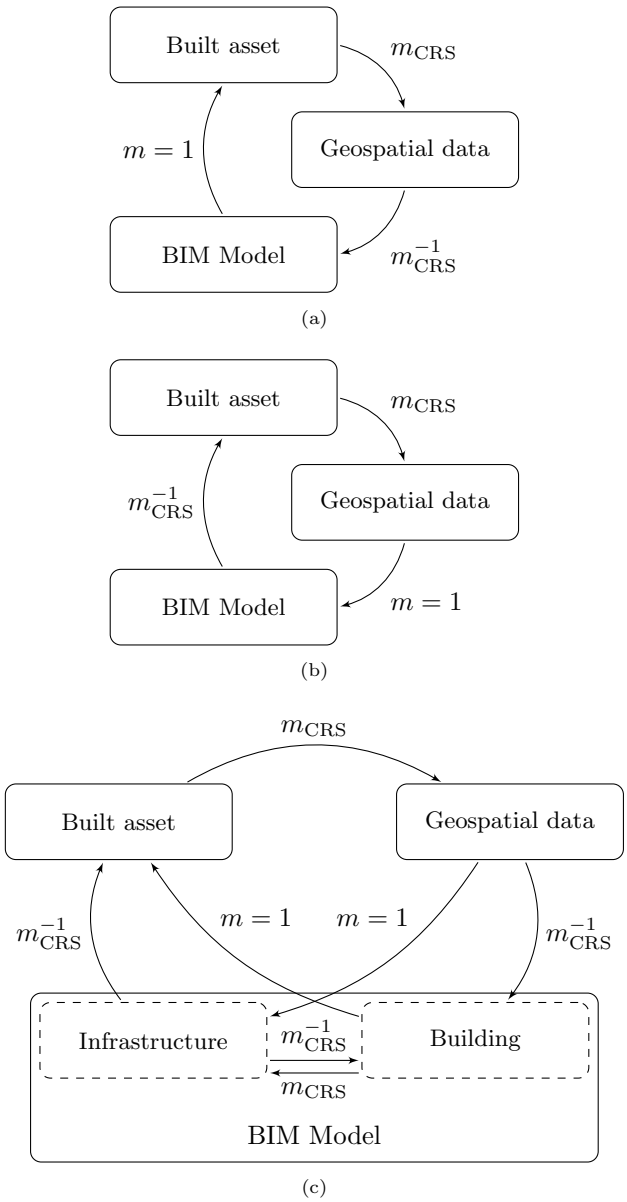

Figure 13: Different options for transforming the data following the information flow from Figure 1: (a) Option A with $m_p = 1$, (b) Option B with $m_p = m_{\mathrm{CRS}}$, and (c) Option C as a combination of Options A and B. These are the different interpretation of the project scale, m_p, of BIM models discussed within this paper. Options A and B differentiate in the step where m_{CRS}^{-1} is applied. Option C is a combination of the two, where buildings are considered according to Option A and infrastructure objects according to Option B. Notice the necessary transformation of data between the BIM models from different fields in Option C.

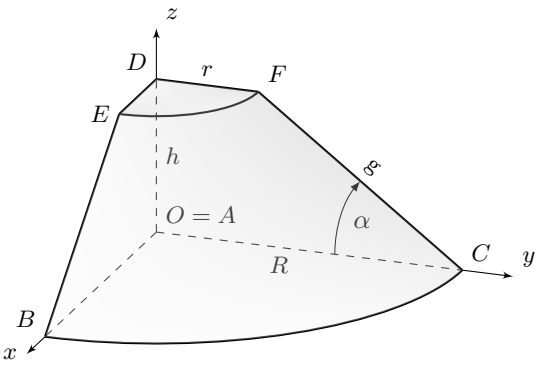

Figure 14: The dimensions of the embankment with marked POO and coordinate axes (not to scale).

The expected result on the construction site should have the required dimensions (Figure 14):

- the top radius, $r = 1\,\mathrm{m}$,
- the height of the embankment, $h = 10\,\mathrm{m}$, and
- the slope of the embankment, $1 : 2$, i.e. $g = 50\,\%$ or $\angle ABE = \angle ACF = 26.6^\circ$.

From these parameters others can be derived. For example, the radius at the bottom of the embankment is $R = r + h/g = 21\,\mathrm{m}$.

Consider an engineer who would like to produce a bill of quantities, and thus needs an exact calculation of the volume of the material needed for the construction of such an embankment. The volume of the frustum in Figure 12 can be calculated using the parametric formula:

$$V = \frac{1}{4}\frac{\pi\, h}{3}\left(R^2 + R\, r + r^2\right) \tag{9}$$

$$= \frac{\pi\, 10}{12}\left(21^2 + 21 \cdot 1 + 1^2\right) = 1212.131\,\mathrm{m}^3\,. \tag{10}$$

On the other hand, the volume of any manifold, non-intersecting and triangulated polytope without borders (e.g. the dotted lines in Figure 11b) can be calculated using the 3D version of the Shoelace formula [6, 38]:

$$V = \frac{1}{6}\sum_{i=1}^{N} \det(P_1^i, P_2^i, P_3^i) = \frac{1}{6}\sum_{i=1}^{N} \begin{vmatrix} x_1^i & x_2^i & x_3^i \\ y_1^i & y_2^i & y_3^i \\ z_1^i & z_2^i & z_3^i \end{vmatrix}, \tag{11}$$

where N is the number of triangles and P_j^i represents the coordinates of the i^{th} triangle's j^{th} vertex and is defined by

$$P_j^i = [x_j^i, y_j^i, z_j^i]^T \quad \forall i \in \{1, \ldots, N\}, \forall j \in \{1, 2, 3\}\,. \tag{12}$$

Table 4: The calculated volumes of the different geometric representations of the frustum in Figure 14 following Section 3.2.2. Its correct volume is derived in Equation (10).

	Geometric representation				
	explicit		implicit		
	Tessellation	BRep	Extrusion	CSG	Unit
Volume	1157.500	1200.649	1212.131	1212.131	m^3
	95.49	99.05	100.00	100.00	%
Figure	11b	11a	12a	12b	

The vertices in each triangle need to be provided in counter-clockwise order, as seen from the inside of the solid.

Table 4 shows the differences in volume between the different geometric representations.

4.2.2. Road

Since the geodetic distortions depend on the location of the asset on the Earth, we consider a 10 m wide road going through four different locations within the state of Bavaria. The road begins just shy of the western border of Bavaria, at the southern-most point of the Lake *Gustavsee*, near the city of Seligenstadt. It runs to the east until it crosses the town of Bayreuth, where it turns south on the campus of the University of Bayreuth. In the centre of Munich, in front of the main entrance to the Technical University of Munich, it turns eastwards again. The road ends at the eastern border of the state of Bavaria, where Germany, Austria and the Czech Republic meet. The corresponding indices of the prominent locations are *west*, *byu*, *muc* and *east*, respectively.

Because of the huge difference in the sizes of the Earth and the road, a true-to-scale representation would exceed the precision of a pixel on printed medium. This is why, Figure 15 shows the road only schematically, where the road is shown on the ellipsoid and in the Cartesian PCS. The geodetic parameters for transformation between the curved and projected representations are provided in Tables 5 and 6.

As is usually the case in infrastructure projects, the PCS and the CRS coincide, $(X, Y) = (E, N)$, and all geometry representations have 'big' coordinate values, i.e. geodetic coordinates[12]. The distortions induced by UTM map projection at a particular location on the (X, Y) plane (i.e. the (E, N) plane) can be calculated according to Equation (A.10).

The road can be treated if it were split into three segments[13]. The first

[12]Many (architectural) modelling software suites chose to only allow models to reside close to the POO of the PCS. Reasoning behind this is the computational stability of digital representations of decimal numbers when only single precision arithmetic is used [see also 9]. As such, these programs encounter problems when BIM models are imported with – although valid – "big" coordinates. However, as far as modelling as a concept is concerned, this does not represent any obstacle.

[13]Euclidean geometry holds in BIM models per definition of the PCS. On Earth, it holds in

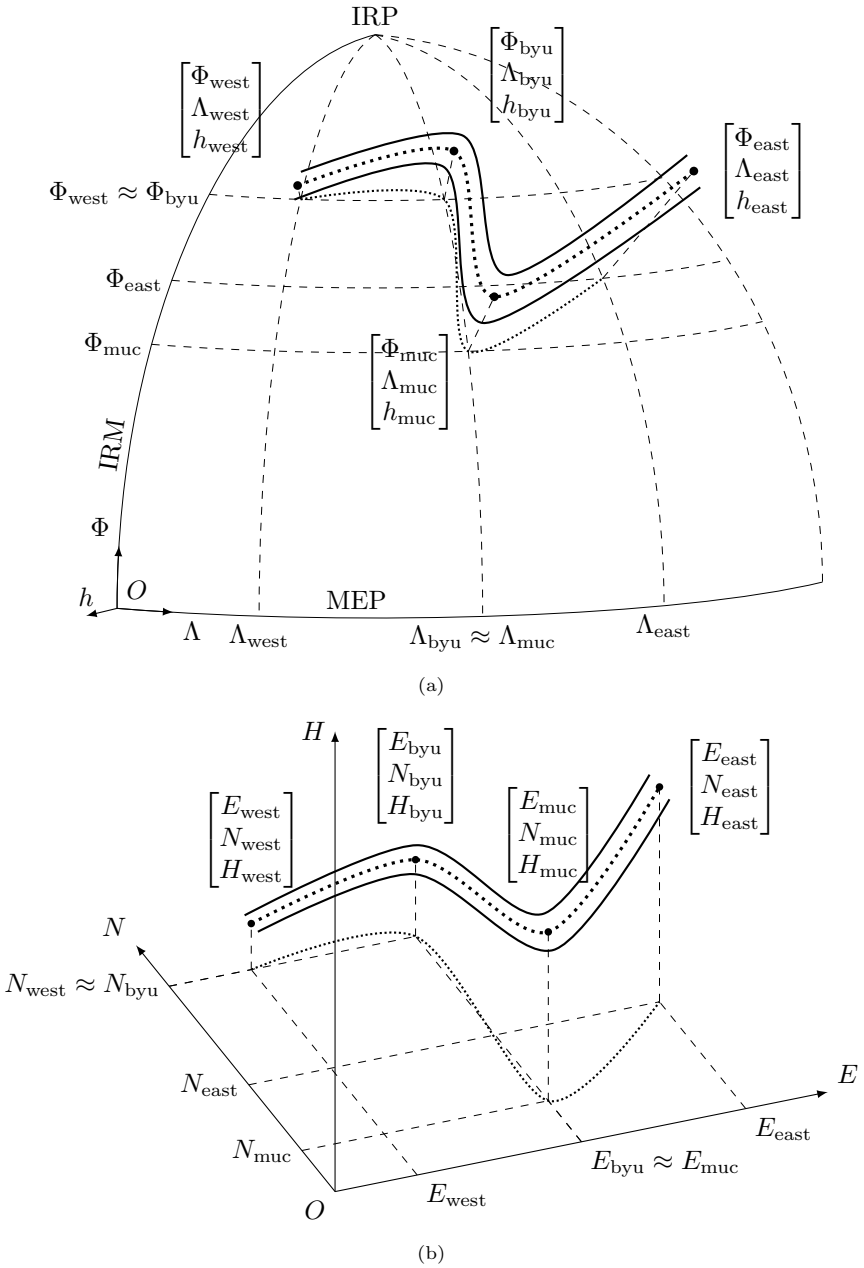

Figure 15: The road example with schematic representation of the four location (not to scale): (a) on the ellipsoid and (b) in the PCS. The exact values of coordinates are provided in Table 6.

Table 5: The parameters of the CRS for all four locations needed for geodetic transformations.

Parameter	Value
Geodetic datum	ETRS89
EPSG code	6258
Ellipsoid	GRS80 1980
EPSG code	7019
R_{major}	6 378 137.0 m
f^{-1}	298.257 222 101
Vertical datum	DHHN 20162016
EPSG code	1170
Map projection	UTM
zone	32N
Λ_0	9°0′0″
EPSG code	25832
E_0	500 000 m
N_0	0 m

Table 6: The parameters of the different locations needed for geodetic transformations. m_{CRS}, m_{proj} and m_h are calculated according to Equations (7), (A.10) and (A.14), respectively.

Parameter	*west*	*byu*	*muc*	*east*
Ellipsoidal coordinates				
Φ	N50°03′02.770″	N49°55′43.693″	N48°08′54.899″	N48°46′17.541″
Λ	E08°59′29.545″	E11°35′09.047″	E11°34′06.888″	E13°50′22.080″
Projected coordinates and scale				
E[a]	499 394.35 m	685 582.84 m	691 046.73 m	855 531.47 m
N	5 544 275.53 m	5 533 920.52 m	5 336 005.65 m	5 413 364.53 m
m_{proj}	0.999 600 0	1.000 023 0	1.000 048 5	1.001 152 9
Elevation coordinates and scale				
h	104.0 m	352.0 m	515.0 m	1321.0 m
H	56.15 m	305.37 m	469.34 m	1274.00 m
U	47.85 m	46.63 m	45.66 m	47.00 m
m_h	0.999 983 7	0.999 944 8	0.999 919 3	0.999 793 0
CRS scale at (Φ, Λ, h)				
m_{CRS}	0.999 583 7	0.999 967 8	0.999 967 7	1.000 945 6
Δ_{CRS}	−416.3 ppm	−32.1 ppm	−32.3 ppm	945.6 ppm

[a] In some cases, these coordinates are prepended with the zone number, in our case that would be 32xxxxxx.xx.

segment, *west–byu*, lies between the meridian and the intersection of the UTM projection cylinder with the ellipsoid which lies approximately at Bayreuth. Here, the projection is shortening the real distances (observe m_{proj} in Table 6). The second segment, *byu–muc*, runs almost along the intersection line, where very little distortion occurs. The third and last segment, *muc–east*, lies between the intersection line and the border, extending over the usual boundary between zone 32 and zone 33 (at 12°) to 13.8°. Here, the UTM projection lengthens the real distances (Figures 9 and 10a).

In AEC design, the distance between two points is often important. On the one hand, the distance between two points $|P_1P_2|_\angle$ in the projected CS can be calculated as

$$|P_1P_2|_\angle = \sqrt{(x_2 - x_1)^2 + (y_2 - y_1)^2}\ . \tag{13}$$

On the other hand, the distance between two points $|P_1P_2|_\circ$ on the ellipsoid (also called the geodesic) can only be calculated iteratively in the general case. The calculation of the inverse geodesic is complex [described in full by 29]:

$$k = e' \cos\alpha_0 \tag{14}$$

$$I(\sigma) = \int_0^\sigma \sqrt{1 + k^2 \sin^2\sigma'}\, d\sigma', \tag{15}$$

$$|P_1P_2|_\circ = \frac{I(\sigma_2) - I(\sigma_1)}{b}, \tag{16}$$

where α_0 denotes the azimuth of the geodesic at the Equator and σ_1 and σ_2 are the spherical arc lengths on the auxiliary sphere from the intersection of the geodesic with Equator to P_1 and P_2, respectively [29, Figure 2].

The comparison of the distances from Equations (13) and (16) for each segment is shown in Table 7. As expected, the difference between the on-site and ellipsoidal distances corresponds to the height reduction from Section 3.1.4, while the difference between the ellipsoidal and projected distances corresponds to the properties of the UTM projection from Section 3.1.5. In the first segment, *west–byu*, each meter in the model is on average shorter by about 0.30 mm compared to on-site measurements, whereas in the third segment, *muc–east*, each meter in the model is on average roughly 0.40 mm longer than that on the site. These values are the averages along the whole length of that segment; in reality, they change with varying m_{proj} and m_h, as calculated from Equations (A.5) and (A.14), respectively. For example, compare averages of Δ_{CRS} from Table 6 with the corresponding differences $d_{\text{proj}}/d_{\text{true}}$ from Table 7.

4.2.3. Railway

The last case study is presented in Figure 2, where a new railway line with four stations is planned. As presented in Section 4, there are three possibilities

close proximity of the observer as noted in Section 1. This is why a split into segments does not infer any modelling obstacles.

Table 7: The comparison of the 2D distances between the on-site locations in Table 6 (true distance), on the ellipsoid using Equation (16); and those in the projected CS using Equation (13). The differences are calculated following Equation (1).

Distance	Expression	*west–byu*	*byu–muc*	*muc–east*	Unit
on site[a,b]	d_{true}	186 531.285	197 996.654	181 695.134	m
ellipsoidal[a]	d_{ell}	186 524.617	197 983.198	181 668.986	m
difference	$d_{\text{true}} - d_{\text{ell}}$	6.668	13.456	26.148	m
	$d_{\text{ell}}/d_{\text{true}} - 1$	−35.747	−67.961	−143.911	ppm
projected	d_{proj}	186 476.218	197 990.277	181 768.056	m
difference	$d_{\text{ell}} - d_{\text{proj}}$	48.399	−7.079	−99.070	m
	$d_{\text{proj}}/d_{\text{ell}} - 1$	−259.476	35.757	545.330	ppm
combined	$d_{\text{true}} - d_{\text{proj}}$	55.067	6.377	−72.922	m
difference	$d_{\text{proj}}/d_{\text{true}} - 1$	−295.214	−32.207	401.340	ppm

[a] Calculated using the GeodSolve calculator [30].
[b] True distances have been calculated using the average elevation between the two points.

for interpreting this BIM model. Recall that Option C is a combination of Options A and B, where some objects are interpreted according to the first and others according to the second option. This is the case in this project, where the stations were developed according to Option A and the railway line according to Option B.

Railway Line. For the railway line, any chosen POO would be equally sub-optimal. The m_p cannot be neglected anywhere, as the railway line runs through all four stations and it changes continuously according to Equations (A.5) and (A.14). Historically, this is the reason that the POO of long infrastructure objects has usually been left as the POO of the projected CRS, which would be $(X_0, Y_0) = (E_0, N_0)$ in our case. With the usage of 'big' coordinate values, all project stakeholders are typically aware of the equality of CRS = PCS [35].

When calculating the set out values, m_{CRS}^{-1} needs to be applied. When exchanging the data between the models of stations and of the railway, it needs to be converted accordingly, using m_{CRS} or m_{CRS}^{-1} as marked in Figure 13c. Should this be omitted (forgotten or knowingly neglected) at any point in the process, it could introduce errors that are hard to discover and remediate. This problem is discussed in detail in Section 4.3.

Stations. The four stations are located at the four locations described in Section 4.2.2 as vertices in the *road* case study, and their locations on Earth are presented in Table 6. Since the station's overall size is small compared to Earth, the deviation of a plane from the curved surface is very small ($< 1.25\,\text{cm}$ at 0.4 km distance from POO). Thus, the Earth can be assumed flat in the vicinity of the station's origin.

Before the design, the geospatial data was transformed back to its true form as shown in Figure 13c. Therefore, we can interpret the geometries according to Option A. When the reading software interprets the geometry and produces the

set-out values, or calculates the bill of quantities, the horizontal dimensions do not need to be scaled by the corresponding value of m_p to obtain the dimensions on Earth, but can be used as-is, instead. This approach introduces a certain discrepancy at the borders between the railway line and the stations as discussed in Sections 4.3 and 5.

4.3. Negligence of the Scale Function

If any of the factors is not applied correctly when exchanging data during the project (especially when exchanging BIM models with Option C), certain measurable discrepancies will be introduced between the model and the reality that it models. We show two possible consequences based on the *railway* case study from Section 4.2.3, both depicting the problem which emerges from the lack of (back-)transformation.

4.3.1. Incorrect Volumes

Let us assume that at each of the stations from Section 4.2.3, some sort of embankment for a bridging structure, like the one presented in Section 4.2.1, would be needed. The geospatial data was not transformed by m_{CRS}^{-1} as shown in Figure 13c; rather, it was used as-is in the design process (i.e. distorted). The designer was aware of that and followed Option B when designing the embankments using scaled horizontal dimensions $[rR]^T_{i,\text{design}} = m_{\text{CRS},i}\,[rR]^T$; $\forall i \in \{west, byu, muc, east\}$.

Following the design phase, an engineer would like to produce a bill of quantities and would thus need an exact calculation of the volume of material needed for the construction. However, he interpreted the model according to Option A and thus deducted wrong quantities as presented in Table 8. As shown in Section 4.2.1, different geometric representations imply different volumes. The volumes for all 16 combinations (4 representations $\times$ 4 locations) are presented in Table 8, where the clear influence of the geodetic transformations can be seen. The correct volumes of the different geometric representations are provided in Table 4, as a reference.

To calculate the volumes in Table 8, we assumed a constant underlying scale m_p, because of a very small change in the scaling factor $|\Delta_l - \Delta_{l+20}| < 0.1\,\text{ppm}$. We applied $\lambda = m_p = m_{\text{CRS}}$ from Table 6 to the horizontal axes of the PCS. For that, Equation (3) cannot be used as is, but needs to be changed to the following (notice the position of λ):

$$\begin{bmatrix} u_i \\ v_i \\ w_i \end{bmatrix} = \begin{bmatrix} t_u \\ t_v \\ t_w \end{bmatrix} + R(0,0,\gamma) \begin{bmatrix} \lambda x_i \\ \lambda y_i \\ z_i \end{bmatrix} \quad . \tag{17}$$

4.3.2. Broken Continuity

Consider the railway with a station from Section 4.2.3, whose design process and resulting (mis-)interpretations are shown in Figure 16. The real-world grid of distances on the construction site is shown in Figure 16a, together with two compulsory points denoting the existing railway with its outgoing directions. First, the construction area was surveyed and the current state of the site was scaled down, as seen in Figure 16b. For the sake of simplicity, the m_{CRS} was

Table 8: The calculated volumes of the geometric representations from Figures 11 and 12 for all four locations, where they were designed following Option B, but interpreted according to Option A. The base-line references are presented in Table 4 and Equation (10). Note, that m_{CRS} is only applied to the horizontal axes.

		Geometric representation				
		explicit		implicit		
		Tessellation	BRep	Extrusion	CSG	
Location	*west*	1156.536	1199.649	1211.122	1211.122	m^3
		95.41	98.97	99.92	99.92	%
	byu	1157.425	1200.572	1212.053	1212.053	m^3
		95.49	99.05	99.99	99.99	%
	muc	1157.425	1200.571	1212.053	1212.053	m^3
		95.49	99.05	99.99	99.99	%
	east	1159.690	1202.921	1214.425	1214.425	m^3
		95.67	99.24	100.19	100.19	%

assumed to be constant for the whole construction site[14]. At the projection plane in UTM coordinates, for example, the railway line was designed using Option B, with a representative (mean) scaling factor $m_p < 1$.

The line sections were used *as-is* to design each station. However, the corresponding engineer misinterpreted the model to be in the scale $m_p = 1$ (i.e. according to Option A; Figure 16c). Following Figure 13c, the surroundings of the stations were shortened by the underlying CRS to the model and thus the railway platform was designed on shortened base data. The platform, in turn, used prefabricated elements derived directly from the BIM model, still following the Option A. The surveyor was instructed of that fact and set out the station to be $m_p = 1$ with the model in order not to interfere with the prefabrication processes. Thus, the railway line within the station does not match the design intent of the railway engineer; instead, it deviates from it by a factor of m_{CRS} (Figure 16c).

Misinterpretation due to neglect or lack of understanding causes divergences from the design, which may cause a break in the continuity and/or smoothness of geometries. If we keep the tangent direction of the railway track and the neighbouring railway platform the same, then the track *leaving* the station will not connect to the track of the free route *leading into* the station without a measurable discontinuity. If the surveyor were to set out the free route of the railway strictly following m_{CRS}^{-1}, then the two tracks would not meet at the station's edges (Figure 16d). Thus, it is necessary to introduce a transition zone between the two spatial references, which results in additional considerations during the design and construction processes. The extent of this zone and parameters used are decided by the surveyor responsible for setting out and, to the authors' best knowledge, currently cannot be represented in any BIM model or standard data formats like IFC.

[14]Following that, it is irrelevant, where the identical point resides; depicted is the middle of the station. In the general case, none of these assumptions holds true; see Equation (7).

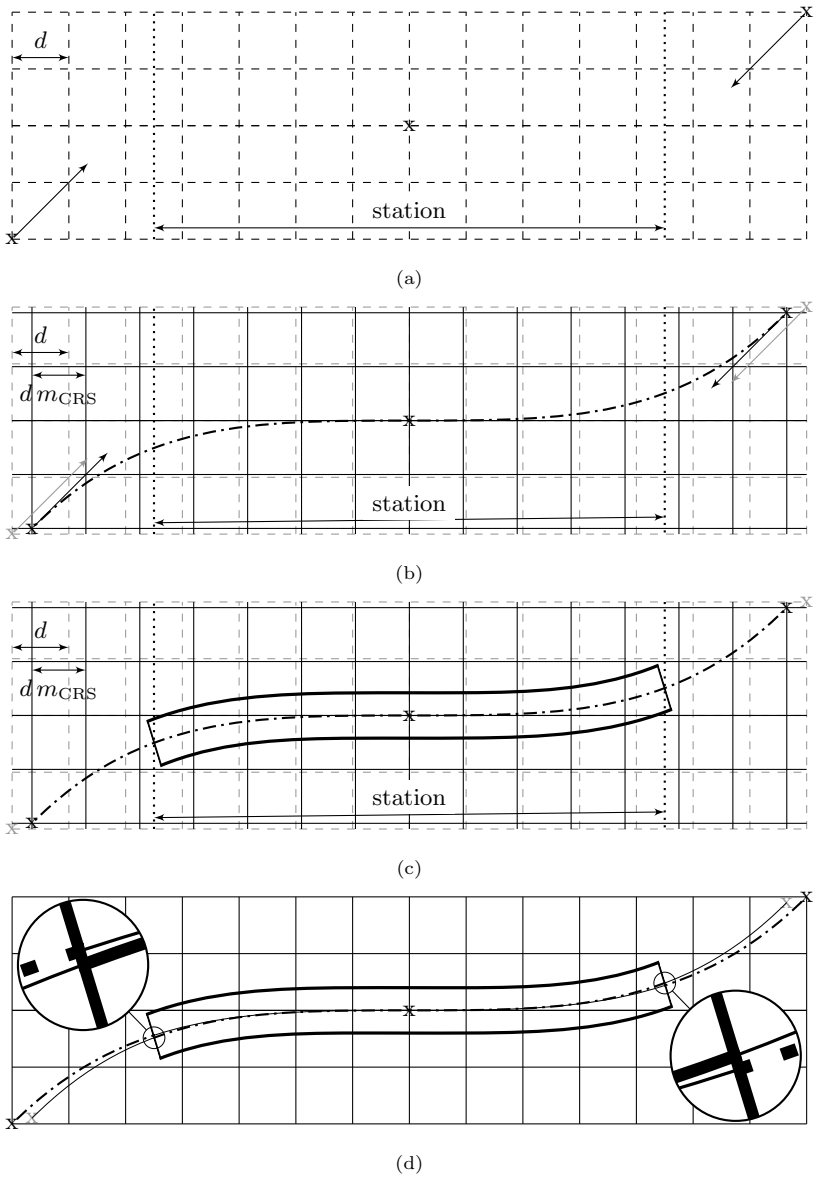

Figure 16: Visualisation of missing transformations from Figure 13c between infrastructure and building models, and their consequences on the example of a station from Figure 2. (a) Grid of the nature with cell length d together with marked design parameters for a railway station. The compulsory points (X) and track directions at the border of the construction site are marked, as well as desired station's length l_{station}. (b) The construction site is surveyed and the grid scaled by CRS is produced ($d\,m_{\text{CRS}}$) with its centre at the central compulsory point (surveyor's decision, it could have been anywhere else as well). The scaling factor is set to $m_{\text{CRS}} = 0.95$ and assumed constant for the whole construction site in order to better visualize the scenario. Here, the track engineer then designs the track alignment as shown with dash-dot line. (c) The station engineer now takes the alignment without scaling it back with m_{CRS}^{-1} and designs the railway station parallel to it. (d) Setting out the station as designed by option A and the track as option B results in discontinuity of the main alignment at station's ends (see zoom-ins at the edges). Not accounting for this when setting out the free route track would result in a *jump* in the track, which is not acceptable. This is why a transition zone needs to be introduced where the track is additionally distorted to fit into the station.

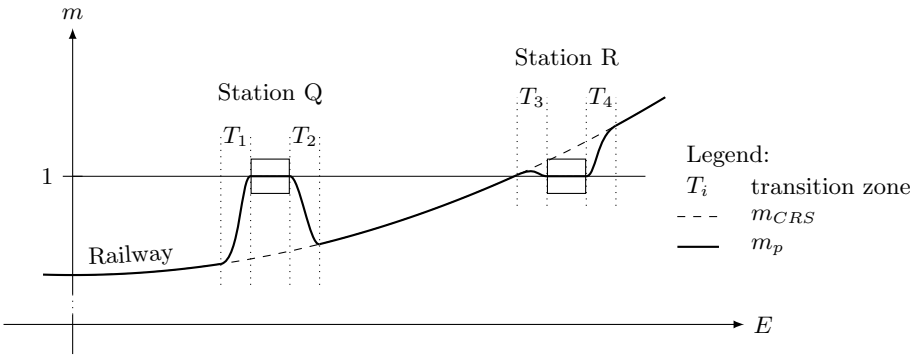

Figure 17: The BIM model from Figure 2, interpreted according to Option C. The stations are interpreted according to Option A and thus have a constant scale, $m_p = 1$, for the whole structure. The railway line is interpreted according to Option B with a continuously changing scale, $m_p = m_{CRS}$ (the representation is simplified to be only dependent on the Easting coordinate from UTM). The disagreement induced by this needs to be smoothed out in the transition zones (marked with T_i) between the two interpretations. Here, the transition follows a twice-derivable function for steadiness reasons.

Figure 17 depicts this problem for our case study. The project scale, m_p, used at stations Q and R, is depicted together with the one used throughout the railway track as an example. As mentioned above, the BIM models of the stations are interpreted according to Option A, with $m_p = 1$. The track is interpreted according to Option B, and thus the project's scale follows the underlying scale of CRS, $m_p = m_{CRS}$. Between the two interpretations, the transition zones, T_i, need to be defined where m_p follows some function of m_{CRS}:

$$\forall T_i : m_p = f_i(m_{CRS})\,. \tag{18}$$

For example, the transition zones in Figure 17 show these functions to be C^2 continuous.

With this constellation, the BIM models of the stations have been designed using distorted geospatial data, but they are interpreted according to Option A. The BIM model of the railway line has been designed with an Option B interpretation. This induces a discontinuity in the transition areas, which requires some accommodation. The strategy most commonly used is to steadily 'brush off' the differences, as shown in Figure 17. The line and the stations in the Figure lie purely in the East-West direction. Of course, circumstances can be more complicated in the nature, where, in addition to the North-South direction, differences in ellipsoidal heights also play an important role (see Equation (7)).

5. Discussion

5.1. The Root of the Problem

We discussed in Section 3.1 how geodesy models the Earth. In Section 3.2, we described how the AEC domain bases the model on the design steps needed to produce it. Both approaches yield information models, but on a different basis. These different approaches are rooted in the historical development and base philosophies of the two disciplines [11, 28]. This difference in modelling

paradigm can be best addressed with two questions that are derived from Figure 1.

The geodetic world primarily answers the question: '*what can be seen there and how can it be captured?*' It tries to encode the state of the Earth, and thus the construction site, as it resides in the present. Surveyors model what can be measured on the Earth in a *bottom-up* manner. The objects' top surfaces are reconstructed from observations of individual points (*bottom*), which are then connected to form increasingly rich semantic entities, geometries and relationships (*up*).

The BIM world primarily answers the question: '*how should that object be designed and how can that information best be transferred?*' That is, the designers imagine objects that do not yet exist, and thus still need to be transposed from concept to reality. AEC experts design in a *top-down* manner, and that is how the model is constructed. The idea of the structure is, at first, only vaguely represented with simple geometries and semantics (*top*) [2]. The model is then refined in later design stages (*down*), with increasing levels of detail until it is finally erected at the construction site from a complete model [28].

Both worlds have developed their own methods and models, which require care to merge and clear definition to transform. The core problem is the completely different definitions of the (E, N) and H coordinate axes in the geospatial world, which is contradictory to the equality of the Cartesian axes (X, Y, Z) in the BIM world [36]. This leads to a deceptively simple question at the intersection of geodesy and design: '*How should we set out the objects on the construction site?*' This difference must be adequately addressed by the whole community in order to minimise the possibility for misunderstandings and potentially costly errors.

5.2. Interpretation

In Section 4, we presented three options for how to interpret digital models, and Table 9 shows how these models are usually interpreted. Clearly, anything surveyed is transformed with m_{CRS} of the underlying CRS in the geospatial domain. The interpretation of a BIM model is not as straight-forward as also implied by Table 1.

On the one hand, Option A sees the model as being a 1:1 copy of the real asset, as is prevalent in the building sector where the structure's extents are rather small (Figure 13a). Table 1 shows that BIM models are mostly interpreted in this manner in the literature. In our opinion this stems from the fact that BIM had its roots in building design and has only recently been introduced to the infrastructure sector [e.g. 3]. As such, the vast majority of research has been focused on buildings.

On the other hand, Option B interprets the model as distorted according to the underlying CRS, which is prevalent in the infrastructure sector [e.g. 34] and is the *de-facto* norm in GIS [33]. If this is the correct choice for a project, then combining GIS and BIM data is easily achieved as long as both are in the same CRS. Considering that different kinds of geospatial data, like DTM or property borders, must be referenced during the alignment design, there is no realistic alternative to Option B for any kind of infrastructure project.

Table 9: The prevalent interpretations of buildings and infrastructure objects on blueprints or in models within the corresponding disciplines (Table 1).

Object	BIM	Geospatial
Building	Option A	Option B
Infrastructure	Option B	Option B
Combination	Option C	–

Option C combines both approaches, interpreting parts of the model according to Option A, while other parts follow Option B. This option is prevalent for models of small infrastructure objects (like short bridges or railway stations), where the structure itself is *small* (Option A), but is integrated into a larger system (Option B).

5.2.1. Why does it Matter?

What are the consequences of falsely interpreting a distorted model as undistorted, or vice-versa? What happens if there was no back-transformation of geospatial data before the design process started for buildings, as presented in Figures 13a and 13c? Under these conditions, the designs (Option A) were based on still-distorted data and thus cannot be set out in the real world without introducing some discrepancy between the objects, as shown in Figure 16. For example, direct prefabrication from a BIM model can lead to finished products that do not exactly fit in their prescribed places. In the same manner, imagine a contractor ordering $(100 \pm 5)\,\%$ of the material needed, as shown in Table 8, just by using the volumes directly from the design model, and not accounting for the distortions introduced by the underlying CRS. This kind of mistake can be hard to spot, as it is an absence of a step in the process, rather than an included step that is wrong.

Another example is a norm that prescribes at least d_{norm} clearance between the façade of a building and the centreline of the railway track. Because the designers know the geospatial data used in the design possesses a certain scale factor, $m_{\mathrm{CRS}} < 1$, they use the scaled-down value for this distance ($d_{\mathrm{norm,CRS}} = m_{\mathrm{CRS}}\ d_{\mathrm{norm}}$) following the interpretation in Option B. They then design the building as close as possible to the railway line, with $d_{\mathrm{design}} = d_{\mathrm{norm,CRS}}$. Code-compliance checking software considers the BIM model according to Option A and reports an error because $d_{\mathrm{design}} < d_{\mathrm{norm}}$. As shown above, that is of course not the case, but pin-pointing the source of this discrepancy could prove to be very cumbersome.

Similarly, imagine the radius of a railway curve, $R_{\mathrm{design}} = 1000\,\mathrm{m}$, resulting in an $R_{\mathrm{real}} = 1000.5\,\mathrm{m}$ at the construction site. The discrepancies in geometry between the design coordinates and the set-out values (because of the application of m_{CRS}^{-1}) influence the driving dynamics insignificantly. However, the change in position could result in a violation of a compulsory point's margin, such as a railway platform's edge, if not handled correctly [20]. If the railway line model were to be interpreted according to Uggla and Horemuz [48], the discrepancies

would be $\Delta = 81\,\text{ppm}$ at 140 km from the POO[15].

5.2.2. Which Option to Use?

Option A considers the models to conform to $m_p = 1$ with the real asset. If geospatial data was not used as input for the model, or if it was used and scaled back to its natural dimensions by m_{CRS}^{-1} according to its underlying CRS (Figure 13a), this option can still hold true.

Additionally, if the model has been designed based on only one spatial reference point (e.g. one cadastral point with its elevation), then this option is viable. The set-out can be based on this point, with the dimensions provided by the BIM model. This represents the topocentric system described in Section 3.1.2, which is the interpretation used by Uggla and Horemuz [48]. In this case, the POO of the PCS represents the POO of the topocentric (right-handed) CRS. This is, however, only valid within a small area around the POO, as described previously.

Option B considers the models distorted according to the underlying CRS, as $m_p = m_{\text{CRS}}$ (Figure 13b). In this case, the geometries in the BIM model are, in principle, not equivalent to their real-world counterparts in either size, shape or relative position. If the geodetic parameters, as described in Section 3.1, are chosen correctly, this equality may be achieved to a certain extent. For example, the custom CRS of the Brenner Basis Tunnel was designed so that the meridian of the projection runs along the main alignment of the tunnel, thus making the scaling factor of the projection $m_{\text{proj}} \approx 1$ within the project's area. As the zero height level was set to the mean terrain height, it yielded a value of $m_h \approx 1$, and thus $m_p = m_{\text{CRS}} \approx 1$ following Equation (7). After defining such a custom CRS, any geospatial data relevant for the project must be transformed into the newly defined CRS [35].

This discrepancy between the model and the real world may be hard to grasp, but is very important, especially if code-compliance checking or direct prefabrication systems use the BIM model as their primary source of design data [e.g. 31]. Additionally, this needs to be properly addressed if data from BIM and GIS models are to be linked or transformed between each other [e.g. 39, 42]. For that, the dimensions and rules need to be carefully adjusted using the scale factor induced by the underlying CRS.

Option C combines the other two options, applying option A to buildings and Option B to infrastructure objects (Figure 13c). This option is ambiguous, because a cut-off must exist to answer the question, '*which objects are to be interpreted according to Option A and which to Option B?*' Heunecke [20] notes that this limit depends on the precision requirements and tolerances of the construction of the 'small' structures involved. A more specific phrasing of this question would be '*what degree of distortion induced by CRS can be neglected while still achieving the requested results?*' We provide an answer to these questions in the following section.

[15] However, their calculations do not take into account the non-spherical shape of the Earth, or that locations on the ellipsoid have different rates of curvature depending on location (see Equations (A.11) and (A.12)), which would complicate their calculations.

5.2.3. Correct Borderline Interpretation

Sections 4.3 and 5.2.1 discussed some of the consequences of a false interpretation of a BIM model. These depend on the required construction precision and the specific geospatial data used during the design. Brenner et al. [8] produced a nomograph (Figure 18) that allows for a determination of the maximal horizontal extent of a structure, depending on the distortion Δ_{CRS} of the underlying CRS and the prescribed construction precision. This reflects false interpretation *by choice* and needs to be addressed adequately by all stakeholders within a project.

Consider the 10 m wide road from Section 4.2.2 constructed to a precision of 1 cm. Its maximal horizontal dimensions cannot exceed about 22 m, 330 m, 330 m and 11 m at the four locations, respectively (given the CRS defined in Table 5 and the distortions provided in Table 6). This means that when setting out the lateral extent of the road, one can knowingly neglect the discrepancies between the model and the reality, since its width is smaller in all four cases. However, when setting out the longitudinal extent of the road, one *cannot* use BIM data without (back-)transformation.

5.3. Recommendations

5.3.1. Process of Interpretation

Generally speaking, if project participants transformed their data strictly according to Figure 13, any option presented in this paper can be viable. Additionally, interpreting any BIM model according to option B will always be correct, bearing in mind that the dimensions in the real world may not be the same as in the model (perhaps longer; perhaps shorter). Figure 18 provides the means to determine the maximal horizontal extent of the model below which the distortions of the CRS can be neglected.

The flow chart in Figure 19 shows the interpretation process of a BIM model, where the intended usage is uncertain. First, a distinction is drawn if the BIM geometry has been produced on the basis of any (projected) geospatial data. If there were multiple reference points taken into account (e.g. DTM, neighbouring buildings, streets or geodetic reference points), then the design model needs to be interpreted according to Option B, i.e. being distorted by the underlying CRS of the reference data with m_{CRS}. If such a model were set out according to Option A, some reference points would lie differently compared to the model, so the distance to some reference points may be shortened or elongated. The other option is a geometry based on only one 3D-point – using fewer points would be building castles in the sky.

Next, the maximum horizontal extent of the model needs to be determined from Figure 18, using the project scale factor, Δ_{p}, and the prescribed construction precision. If the dimensions in the model exceed the maximum horizontal extent, the model needs to be handled according to Option B. Otherwise it *may* (though not always) be interpreted as Option A.

5.3.2. Transition Zones

The necessity for transition zones emerges because of the lack of (back-)transformation between infrastructure and building BIM models (cf. Figure 13c). For illustration, consider a bridge constructed to a precision of 1 cm in Munich,

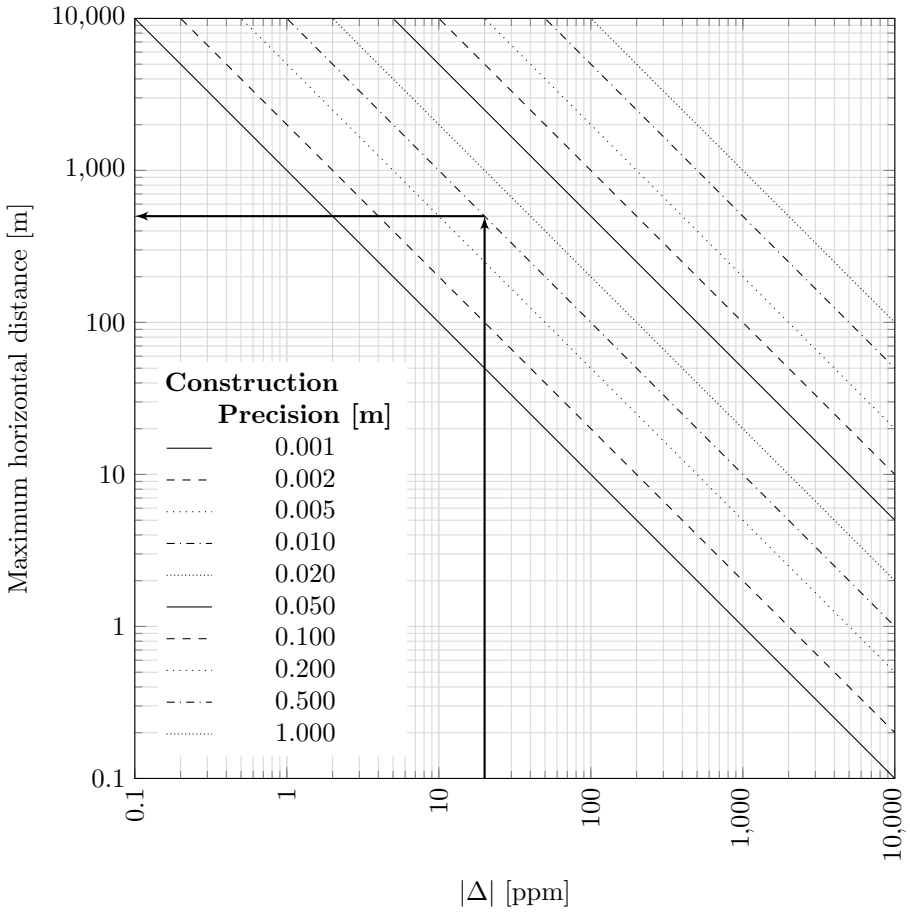

Figure 18: A nomograph to determine the maximum horizontal extents of a structure, depending on the distortion of the underlying CRS, Δ, and the required level of precision of the end structure [redrawn with permission from 8]. For example, the maximum horizontal extent for a construction site with $\Delta = 20\,\text{ppm}$ and a required construction precision of 1 cm is 500 m, as indicated with black arrows.

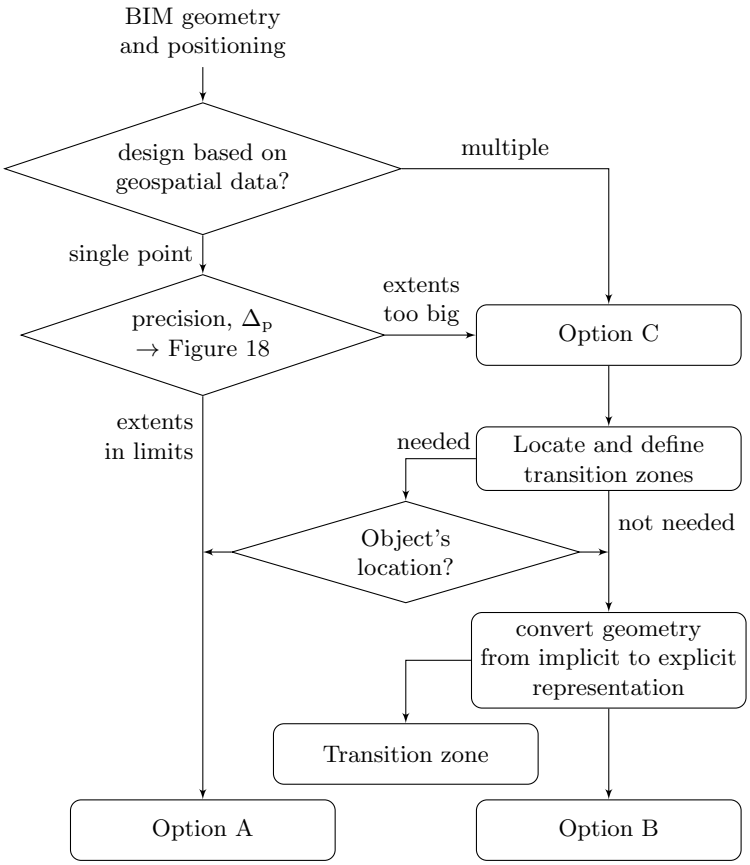

Figure 19: A proposed decision tree to determine the correct interpretation of the geometry within a BIM model.

Germany. Its maximal horizontal dimensions cannot exceed about 350 m, given the CRS defined in Table 5. Up to this extent, engineers could knowingly neglect the implications of the CRS within the BIM model, and still be within the given tolerances. However, the road (or railway) alignment running along the bridge would be incorrectly distorted. Instead of calculating the dimensions using the m_{CRS}^{-1}, they would be interpreted as $m_p = 1$ from the distorted model, thereby inducing an additional discrepancy between the model and the real world at bridge's ends. These discrepancies would need to be smoothed out in the transition zones, as shown in Figure 17.

We note, that if the BIM data had been handled correctly, there would be no need for transition zones. If the maximum horizontal dimensions of the structure are close to, or overshoot, the maximum allowance, then the transition zones need that much more attention and clear definition among the project partners. If the model should be interpreted according to Option B, but with some exceptions handled by Option A then transition zones should be clearly defined.

We stress again that this disagreement is induced by interpreting the stations, embankments and other objects with small extents according to Option A, although based on scaled geospatial data, while correctly interpreting the rest of the extensive model according to Option B [20]. Here, the position and the extent of the asset play an important role in the approach taken its ramifications. The project scale, m_p, and thus the mismatches in location and geometry, depends on the location of the asset on the Earth. If these models must be merged for clash detection, one needs to be converted to the other in some fashion. Such calculations are complex and are often beyond the scope of clash detection software suites.

5.3.3. Conversion of Geometry

Before interpreting the model according to Option B, however, an additional step must be taken. If there are any implicit geometry representations in the BIM model, these need to be made explicit. Because Equation (7) transforms the coordinates of individual points, only the geometries based on points can be correctly georeferenced and thus transformed back during the set-out process. This comes from the different interpretation of the horizontal and vertical axes in the geospatial world and the equality of all three axes in the BIM world, as noted previously.

In order to be able to scale geometries in only two dimensions, they need to be discretised into points. As mentioned above, geodetic transformations of points result in their different relative position and therefore in a possible change of geometrical shape. Collinear points in a CRS may not be collinear anymore and thus even straight lines need to be tessellated. The density of newly added points on lines can be determined following Figure 18 and is dependent on the required precision as well as on the local properties of the CRS. The maximum horizontal extent determines in this case the maximum distance between any two neighbouring points in the geometric representation.

6. Conclusions

In this paper, we have investigated the geospatial context of BIM models; their PCS and how it is located on the *curved* Earth. We wish to raise awareness in the AEC community about this problem, which has previously been addressed entirely within the geospatial domain. We hope that this paper serves as a bridge between the geospatial and BIM worlds by bringing together the background information of these two fields into a single document. We identified three options for BIM model interpretation in the spatial context: the model is either distorted according to the underlying geospatial data or not, or it is a combination of the two. We have presented a case study for each of these options in Section 4.2, which depicted the philosophy behind each interpretation.

As long as construction crews use any levelled instruments at the construction site to determine equal elevation (e.g. spirit levels), we need to account for the fact that the water follows the equipotential surface around the Earth. As shown in Section 2 and Table 1, georeferencing systems have been indecisive with no clear consensus in the literature for how models should be designed and realised. Accurate and unambiguous georeferencing is critical for correct quantity take-offs, automated building and other processes [40]. We stress that a BIM model can represent any construction project, whether in the building or infrastructure sectors. Additionally, this applies to all BIM models, whether they are stored in open data formats like IFC or CityGML, or vendor-specific proprietary models.

We argue that all three options are viable in the AEC industry and none of the options in Table 9 need to be changed. Countless projects have been executed successfully with this approach, and it need not be changed. The BIM models, which are still maturing, need to account for the different possibilities occurring in the industry and not the other way around. They should provide a clear data format in order to circumvent any future disputes about the meaning of saved information. Following that, a recommendation was formulated in Section 5.3. Our primary conclusions are:

1. We join the call of buildingSMART International [10] for increased communication between all participants and the free sharing of information. The processes in Figure 1 need to be adequately understood by all stakeholders.

2. There needs to be a clear distinction between a distorted BIM model (Option B) and one that is not (Option A). If this is not known, Figure 19 helps distinguish *small* and *big* BIM models and objects.

3. Interpreting BIM models with a varying factor following Equation (8) needs to be researched more deeply. We have limited our view on individual points and volumes; however, the distortions can be more complex (see Section 5.2).

4. We need to consider the definition of the transition zones from Equation (18), if we are to allow for interpretations as described in Section 4.3 and Figure 16. The data formats (e.g. IFC) need to develop support for the inclusion of transition zone information. The authors are not aware of any BIM format that would allow for such information, at the moment.

Of course, if the project data were handled correctly, there would be no need for transition zones as presented in Sections 4.3 and 5.3.2. That is, if the data were handled following one of the options shown in Figure 13 strictly (no negligence or misinterpretation). However, this is often not the case in practice.

5. Georeferencing is very important for data conversions and data linking between different data formats [e.g. 46]. If all the relevant information were saved in the same ECEF CRS, data exchanges and linking of data would function without a problem, as all geometries would lie within the same global CS. As this is not the case, all data must include additional metadata about the underlying CRS. The linking approaches have to adapt, as well, as the geometries from different models do not necessarily lie in the same CRS. The integration of the various partial models in a project would work seamlessly, at least from a spatial point of view, if every object were provided in the same (ECEF) CRS.

6. We call for fast implementation of CRS transformation abilities in software suites and their wide adoption by the industry. BIM-ready software solutions currently do not model information like changing scale factor and transition zones, to the best of our knowledge. These should offer transformation functionality to the user – there are already some free libraries available that would support this end [e.g. 18, 37, 41].

Acknowledgements

This research was funded by the *Bundesministerium für Verkehr und digitale Infrastruktur* (Federal Ministry of Transport and Digital Infrastructure, Germany), *Obermeyer Planen+Beraten GmbH* and *ProVI GmbH*. The authors gratefully acknowledge their support.

Conflict of Interest

The authors declare no potential conflicts of interest.

A. Mapping

This section describes the mathematics behind the geodetic projections and distortions described in Section 3.1.5. Only individual points can be transformed and thus any curved geometry needs to be discretised to a tessellated geometry before this process can be performed (see Section 3.2.2). Some variables used in the formulae have been defined in Table 2.

A.1. Mapping $(\Phi, \Lambda) \rightarrow (E, N)$

To convert from ellipsoidal coordinates (Φ, Λ) to geodetic coordinates (E, N), the following formulae can be used [44]. All distances are in kilometres and all angles are in radians. These transformations are valid for both GK and UTM projections, which are differentiated only in terms of their value of scale

at meridian m_0 (see Section 3.1.5 and Equation (1)). First, some intermediate values that depend on the chosen ellipsoid are calculated:

$$\begin{aligned} A &= \frac{a}{1+n}\sum_{i=0}^{\infty}\left(\frac{n}{2}\right)^{2i} \ , \\ \alpha_1 &= \frac{1}{2}n - \frac{2}{3}n^2 + \frac{5}{16}n^3 \ , \\ \alpha_2 &= \frac{13}{48}n^2 - \frac{3}{5}n^3 \ , \\ \alpha_3 &= \frac{61}{240}n^3 \ . \end{aligned} \tag{A.1}$$

Additional intermediate variables are defined for easier notation:

$$\begin{aligned} t(\Phi) &= \sinh\left(\tanh^{-1}\sin\Phi - \frac{2\sqrt{n}}{1+n}\tanh^{-1}\left(\frac{2\sqrt{n}}{1+n}\sin\Phi\right)\right) \ , \\ \xi'(\Lambda) &= \tan^{-1}\left(\frac{t}{\cos(\Lambda-\Lambda_0)}\right) \ , \\ \eta'(\Phi,\Lambda) &= \tanh^{-1}\left(\frac{\sin(\Lambda-\Lambda_0)}{\sqrt{1+t(\Phi)^2}}\right) \ , \\ \sigma(\Phi,\Lambda) &= 1 + \sum_{j=1}^{3} 2j\alpha_j\cos\left(2j\xi'(\Lambda)\right)\cosh\left(2j\eta'(\Phi,\Lambda)\right) \ , \\ \tau(\Phi,\Lambda) &= \sum_{j=1}^{3} 2j\alpha_j\sin\left(2j\xi'(\Lambda)\right)\sinh\left(2j\eta'(\Phi,\Lambda)\right) \ . \end{aligned} \tag{A.2}$$

The final formulae for Easting, E, Northing, N and scale, m_{proj}, depending on the chosen ellipsoid, map projection and ellipsoidal coordinates (Φ, Λ), are:

$$E(\Phi,\Lambda) = E_0 + m_0 A\left(\eta'(\Phi,\Lambda) + \sum_{j=1}^{3}\alpha_j\cos\left(2j\xi'(\Lambda)\right)\sinh\left(2j\eta'(\Phi,\Lambda)\right)\right) \ , \tag{A.3}$$

$$N(\Phi,\Lambda) = N_0 + m_0 A\left(\xi'(\Lambda) + \sum_{j=1}^{3}\alpha_j\sin\left(2j\xi'(\Lambda)\right)\cosh\left(2j\eta'(\Phi,\Lambda)\right)\right) \ , \tag{A.4}$$

$$m_{\text{proj}}(\Phi,\Lambda) = \frac{m_0 A}{a}\sqrt{\left\{1 + \left(\frac{1-n}{1+n}\tan\Phi\right)^2\right\}\frac{\sigma^2(\Phi,\Lambda)+\tau^2(\Phi,\Lambda)}{t^2(\Phi)+\cos^2(\Lambda-\Lambda_0)}} \ , \tag{A.5}$$

where E_0 and N_0 denote the false Easting and false Northing, respectively, and Λ_0 is the longitude of the meridian.

A.2. Inverse Mapping $(E, N) \rightarrow (\Phi, \Lambda)$

To convert from geodetic coordinates (E, N) to ellipsoidal coordinates (Φ, Λ), the following formulae can be used [44]. Again, all distances are in kilometres and all angles are in radians, and these equations are valid for both GK and UTM projections. First, some intermediate values that depend on the chosen ellipsoid are calculated (see also Equation (A.1)):

$$\begin{aligned}
\beta_1 &= \frac{1}{2}n - \frac{2}{3}n^2 + \frac{37}{96}n^3 \ , \\
\beta_2 &= \frac{1}{48}n^2 + \frac{1}{15}n^3 \ , \\
\beta_3 &= \frac{17}{480}n^3 \ , \\
\delta_1 &= 2n - \frac{2}{3}n^2 - 2n^3 \ , \\
\delta_2 &= \frac{7}{3}n^2 - \frac{8}{5}n^3 \ , \\
\delta_3 &= \frac{56}{15}n^3 \ .
\end{aligned} \tag{A.6}$$

Additional intermediate variables are defined for easier notation:

$$\begin{aligned}
\lambda_0 &= \begin{cases} UTM: & \text{Zone} \times 6^\circ - 183^\circ \\ GK: & \text{Zone} \times 3^\circ \end{cases} \ , \\
\xi(N) &= \frac{N - N_0}{m_0 A} \ , \\
\eta(E) &= \frac{E - E_0}{m_0 A} \ , \\
\xi'(E,N) &= \xi(N) - \sum_{j=1}^{3} \beta_j \sin\left(2j\xi(N)\right) \cosh\left(2j\eta(E)\right) \ , \\
\eta'(E,N) &= \eta(E) - \sum_{j=1}^{3} \beta_j \cos\left(2j\xi(N)\right) \sinh\left(2j\eta(E)\right) \ , \\
\sigma'(E,N) &= 1 - \sum_{j=1}^{3} 2j\beta_j \cos\left(2j\xi(N)\right) \cosh\left(2j\eta(E)\right) \ , \\
\tau'(E,N) &= \sum_{j=1}^{3} 2j\beta_j \sin\left(2j\xi(N)\right) \sinh\left(2j\eta(E)\right) \ , \\
\chi(E,N) &= \sin^{-1}\left(\frac{\sin\xi'(E,N)}{\cosh\eta'(E,N)}\right) \ ,
\end{aligned} \tag{A.7}$$

where *Zone* denotes the zone of the projection (e.g. UTM32 / UTM33 or GK 2 / 3 / 4, for Germany).

The final formulae are:

$$\Phi(E,N) = \chi(E,N) + \sum_{j=1}^{3} \delta_j \sin\left(2j\chi(E,N)\right) \ , \tag{A.8}$$

$$\Lambda(E,N) = \Lambda_0 + \tan^{-1}\left(\frac{\sinh\eta'(E,N)}{\cos\xi'(E,N)}\right) \ , \tag{A.9}$$

$$m_{\mathrm{proj}}(E,N) = \frac{m_0 A}{a}\sqrt{\left\{1+\left(\frac{1-n}{1+n}\tan\Phi(E,N)\right)^2\right\}\frac{\cos^2\xi'(E,N)+\sinh^2\eta'(E,N)}{\sigma'^2(E,N)+\tau'^2(E,N)}} \ . \tag{A.10}$$

A.3. Vertical Reduction of Horizontal Distances

Because geospatial data is mapped from an ellipsoidal surface to a flat surface, it first needs to be referenced to it and not the geoid. The data is projected on the ellipsoid first which induces additional dimensional distortions (Figure 9) [24, 35]. The scale, m_h, used to reduce a horizontal distance at the terrain elevation $h = H + U$ to the ellipsoid can be calculated as follows [20]:

$$R_M(\Phi) = \frac{a^2 b^2}{\sqrt{(a^2\cos^2\Phi + b^2\sin^2\Phi)^3}} \ , \tag{A.11}$$

$$R_N(\Phi) = \frac{a^2}{\sqrt{a^2\cos^2\Phi + b^2\sin^2\Phi}} \ , \tag{A.12}$$

$$R_G(\Phi) = \sqrt{R_M(\Phi)R_N(\Phi)} \ , \tag{A.13}$$

$$m_h(\Phi,h) = 1 - \frac{h}{R_G(\Phi)} \ , \tag{A.14}$$

where $R_M(\Phi)$ and $R_N(\Phi)$ are the meridional (north-south) and prime vertical (east-west) radii of curvature, respectively; and $R_G(\Phi)$ is the Gaussian radius of curvature of the ellipsoid [20]. Points on the ellipsoid ($h = 0$) do not get scaled. However, to get the necessary ellipsoidal heights, h, we must know the undulations, U, and thus the geoid. The use of H instead of h in Equation (A.14) leads to an incorrect scale factor, m_h (see also Figure 5).

References

[1] Abedallah, R., 2016. The best uniform quadratic approximation of circular arcs with high accuracy. Open Mathematics 14, 118–127. doi:10.1515/math-2016-0012.

[2] Abualdenien, J., Borrmann, A., 2019. A meta-model approach for formal specification and consistent management of multi-LOD building models. Advanced Engineering Informatics 40, 135 – 153. doi:10.1016/j.aei.2019.04.003.

[3] Barazzetti, L., Banfi, F., 2017. BIM and GIS: When parametric modeling meets geospatial data. ISPRS Annals of Photogrammetry, Remote Sensing & Spatial Information Sciences 4. URL:

https://www.isprs-ann-photogramm-remote-sens-spatial-inf-sci.net/IV-5-W1/1/2017/. accessed: 2020-03-29.

[4] Borrmann, A., Amann, J., Chipman, T., Hyvärinen, J., Liebich, T., Muhič, S., Mol, L., Plume, J., Scarponcini, P., 2017a. IFC Infra Overall Architecture Project: Documentation and Guidelines. Technical Report. buildingSMART International. URL: https://www.buildingsmart.org/standards/bsi-standards/standards-library/. accessed: 2020-03-29.

[5] Borrmann, A., König, M., Koch, C., Beetz, J., 2017b. Building Information Modeling – Technology Foundations and Industry Practise. Springer International. doi:10.1007/978-3-319-92862-3. ISBN: 978-3-319-92861-6.

[6] Braden, B., 1986. The surveyor's area formula. The College Mathematics Journal 17, 326–337. doi:10.2307/2686282.

[7] Bradley, A., Li, H., Lark, R., Dunn, S., 2016. BIM for infrastructure: An overall review and constructor perspective. Automation in Construction 71, 139 – 152. doi:10.1016/j.autcon.2016.08.019.

[8] Brenner, J., Mitchell, A., Maier, F., Yockey, M., Pulikanti, S., 2018. Development of 3D and 4D Bridge Models and Plans. URL: https://www.michigan.gov/mdot/0,4616,7-151-9622_11045_24249-485483--,00.html. accessed: 2020-03-29.

[9] buildingSMART International, 2019. Article about IFC coordinate reference systems, and Revit [forum discussion]. URL: https://forums.buildingsmart.org/t/article-about-ifc-coordinate-reference-systems-and-revit/. accessed: 2020-03-29.

[10] buildingSMART International, 2020. User Guide for Geo-referencing in IFC. URL: https://www.buildingsmart.org/standards/bsi-standards/standards-library/. accessed: 2020-03-29.

[11] Clemen, C., Görne, H., 2019. Level of Georeferencing (LoGeoRef) using IFC for BIM. Journal of Geodesy, Cartography and Cadastre 2019, 15–20. URL: https://jgcc.geoprevi.ro/docs/2019/10/jgcc_2019_no10_3.pdf. accessed: 2020-03-29.

[12] Conchúir, D.O., 2016. Great miscalculations: the importance of validating project management assumptions. URL: http://www.engineersjournal.ie/2016/06/28/gmiscalculation-laufenburg-bridge/. accessed: 2019-09-08.

[13] Costin, A., Adibfar, A., Hu, H., Chen, S.S., 2018. Building Information Modeling (BIM) for transportation infrastructure – Literature review, applications, challenges, and recommendations. Automation in Construction 94, 257 – 281. doi:10.1016/j.autcon.2018.07.001.

[14] Derbyshire, Sam, 2012. OblateSpheroid.PNG. URL: https://commons.wikimedia.org/w/index.php?curid=209084. accessed: 2020-03-29.

[15] Donaubauer, A., Kolbe, T.H., (Eds.), 2017. Leitfaden Bezugsystemwechsel auf ETRS89/UTM: Grundlagen, Erfahrungen und Empfehlungen [Guidelines for change of reference system to ETRS89/UTM: Basics, Experiences and Recommendations]. URL: https://rundertischgis.de/publikationen/leitfaeden.html. accessed: 2020-03-29, [in German].

[16] Eastman, C., Teicholz, P., Sacks, R., Liston, K., 2008. BIM Handbook: A Guide to Building Information Modeling for Owners, Managers, Designers, Engineers and Contractors. Wiley Publishing. doi:10.1002/9780470261309. ISBN: 978-0-470-18528-5.

[17] EPSG, 2020. European Petroleum Survey Group. URL: http://epsg.io/. accessed: 2020-03-29.

[18] Evers, K., Knudsen, T., 2017. Transformation pipelines for PROJ.4, in: Technical Programme and Proceedings of the FIG Working Week 2017, Helsinki, Finnland. ISBN: 978-87-92853-61-5, contribution 9156.

[19] GeoBremen, 2015. UTM Abbildung – Informationen und Handlungsempfehlungen [UTM Projection – Information and Recommended Actions]. Geoinformation Bremen Landesamt, Hansestadt Bremen. URL: http://www.geo.bremen.de/sixcms/media.php/13/UTM_Abbildung_Info_Handlungsempfehlung_150611.pdf. accessed: 2019-05-31, [in German].

[20] Heunecke, O., 2017. Planung und Umsetzung von Bauvorhaben mit amtlichen Lage- und Höhenkoordinaten [Design and Realization of Construction Works with Official Plane and Vertical Coordinates]. zfv 142, 180–187. doi:10.12902/zfv-0160-2017. [in German].

[21] Ince, E.S., Barthelmes, F., Reißland, S., Elger, K., Förste, C., Flechtner, F., Schuh, H., 2019. ICGEM – 15 years of successful collection and distribution of global gravitational models, associated services, and future plans. doi:10.5194/essd-11-647-2019.

[22] ISO 10303-42:2019, 2019. Industrial automation systems and integration – Product data representation and exchange – Part 42: Integrated generic resource: Geometric and topological representation. Standard. International Organization for Standardization. Geneva, CH. URL: https://www.iso.org/standard/78579.html. accessed: 2020-03-29.

[23] ISO 16739-1:2018, 2018. Industry Foundation Classes (IFC) for data sharing in the construction and facility management industries – Part 1: Data schema. Standard. International Organization for Standardization. Geneva, CH. URL: https://www.iso.org/standard/70303.html. accessed: 2020-03-29.

[24] ISO 19111:2019, 2019. Geographic information – Referencing by coordinates. Standard. International Organization for Standardization. Geneva, CH. URL: https://www.iso.org/standard/74039.html. accessed: 2020-03-29.

[25] ISO 19162:2019, 2019. Geographic information – Well-known text representation of coordinate reference systems. Standard. International Organization for Standardization. Geneva, CH. URL: https://www.iso.org/standard/76496.html. accessed: 2020-03-29.

[26] Jaud, Š., Donaubauer, A., Borrmann, A., 2019. Georeferencing within IFC: A Novel Approach for Infrastructure Objects, in: Cho, Y.K., Leite, F., Behzadan, A., Wang, C. (Eds.), Computing in Civil Engineering 2019: Visualisation, Information Modelling, and Simulation. American Society of Civil Engineers, Atlanta, Georgia, USA, pp. 377–384. doi:10.1061/9780784482421.

[27] Kaden, R., Clemen, C., 2017. Applying Geodetic Coordinate Reference Systems within Building Information Modeling (BIM), in: Technical Programme and Proceedings of the FIG Working Week 2017, Helsinki, Finland. ISBN: 978-87-92853-61-5, contribution 8967.

[28] Kaden, R., Clemen, C., Seuß, R., Blankenbach, J., Becker, R., Eichhorn, A., Donaubauer, A., Kolbe, T.H., Gruber, U., (Eds.), 2017. Leitfaden Geodäsie und BIM [Guidelines Geodesy and BIM]. URL: https://rundertischgis.de/publikationen/leitfaeden.html. accessed: 2020-03-29, [in German].

[29] Karney, C.F.F., 2013. Algorithms for geodesics. Journal of Geodesy 87, 43–55. doi:10.1007/s00190-012-0578-z.

[30] Karney, C.F.F., 2015. Online geodesic calculations using the GeodSolve utility. URL: https://geographiclib.sourceforge.io/cgi-bin/GeodSolve. accessed: 2020-03-29.

[31] Li, X., Shen, G.Q., Wu, P., Yue, T., 2019. Integrating building information modeling and prefabrication housing production. Automation in Construction 100, 46 – 60. doi:10.1016/j.autcon.2018.12.024.

[32] Liebich, T., Amann, J., Borrmann, A., Chipman, T., Hyvärinen, J., Muhič, S., Mol, L., Plume, J., Scarponcini, P., 2017. IFC Alignment 1.1 Project: IFC Schema Extension Proposal. Report. buildingSMART International. URL: http://www.buildingsmart-tech.org/downloads/ifc/ifc5-extension-projects/ifc-alignment/ifcalignment-conceptualmodel-cs. accessed: 2018-09-29.

[33] Liu, X., Wang, X., Wright, G., Cheng, J.C.P., Li, X., Liu, R., 2017. A State-of-the-Art Review on the Integration of Building Information Modeling (BIM) and Geographic Information System (GIS). ISPRS International Journal of Geo-Information 6. doi:10.3390/ijgi6020053.

[34] Markič, Š., Donaubauer, A., Borrmann, A., 2018. Enabling Geodetic Coordinate Reference Systems in Building Information Modelling for Infrastructure, in: Proceedings of the 17th International Conference on Computing in Civil and Building Engineering, Tampere, Finnland. URL: http://programme.exordo.com/icccbe2018/delegates/presentation/373/.

[35] Markič, Š., Windischer, G., Glatzl, R.W., Hofmann, M., Borrmann, A., Bergmeister, K., 2019. Requirements for geo-locating transnational infrastructure BIM models, in: Peila, D., Viggiani, G., Celestino, T. (Eds.),

Tunnels and Underground Cities. Engineering and Innovation Meet Archaeology, Architecture and Art. Proceedings of the WTC 2019 ITA-AITES World Tunnel Congress (WTC 2019). 1 ed.. CRC Press, pp. 972–981. doi:10.1201/9780429424441.

[36] Nagel, C., Stadler, A., Kolbe, T.H., 2009. Conceptual Requirements for the Automatic Reconstruction of Building Information Models from Uninterpreted 3D Models, in: Kolbe, T.H., Zhang, R., Zlatanova, S. (Eds.), Proceedings of the Academic Track of the Geoweb 2009 - 3D Cityscapes Conference in Vancouver,Canada, 27-31 July 2009, ISPRS. pp. 46–53. URL: http://www.isprs.org/proceedings/xxxviii/3_4-c3/paper_geow09/paper26_nagel_stadler_kolbe.pdf. accessed: 2020-03-29.

[37] NGA, 2019. Mensuration Services Program (MSP) Geographic Translator (GeoTrans). National Geospatial-Intelligence Agency. URL: http://earth-info.nga.mil/GandG/update/index.php. accessed: 2020-03-29.

[38] Nürnberg, R., 2013. Calculating the volume and centroid of a polyhedron in 3d URL: http://www2.imperial.ac.uk/~rn/centroid.pdf. accessed: 2020-03-29.

[39] Ohori, K.A., Diakité, A., Krijnen, T., Ledoux, H., Stoter, J., 2018. Processing BIM and GIS Models in Practice: Experiences and Recommendations from a GeoBIM Project in The Netherlands. ISPRS International Journal of Geo-Information 7, 311. doi:10.3390/ijgi7080311.

[40] Olsson, P.O., Axelsson, J., Hooper, M., Harrie, L., 2018. Automation of Building Permission by Integration of BIM and Geospatial Data. ISPRS International Journal of Geo-Information 7, 307. doi:10.3390/ijgi7080307.

[41] PROJ contributors, 2019. PROJ coordinate transformation software library. Open Source Geospatial Foundation. URL: https://proj.org/. accessed: 2020-03-29.

[42] Sani, M., Abdul Rahman, A., 2018. GIS AND BIM INTEGRATION AT DATA LEVEL: A REVIEW. ISPRS - International Archives of the Photogrammetry, Remote Sensing and Spatial Information Sciences XLII-4/W9, 299–306. doi:10.5194/isprs-archives-XLII-4-W9-299-2018.

[43] Saygi, G., Agugiaro, G., Turan, M., Remondino, F., 2013. Evaluation of GIS and BIM roles for the information management of historical buildings, pp. 283–288. doi:10.5194/isprsannals-II-5-W1-283-2013.

[44] Snyder, J.P., 1987. Map Projections: A Working Manual. Technical Report. Washington, D.C. URL: https://pubs.usgs.gov/pp/1395/report.pdf, doi:10.3133//pp1395. accessed: 2020-03-29.

[45] StackExchange, 2012. How accurate is approximating the Earth as a sphere? URL: https://gis.stackexchange.com/questions/25494. accessed: 2020-03-29.

[46] Stouffs, R., Tauscher, H., Biljecki, F., 2018. Achieving Complete and Near-Lossless Conversion from IFC to CityGML. ISPRS International Journal of Geo-Information 7, 355. doi:10.3390/ijgi7090355.

[47] Torge, W., 1991. Geodesy. Walter de Gruyter & Co. ISBN: 3-11-012408-4.

[48] Uggla, G., Horemuz, M., 2018a. Geographic capabilities and limitations of Industry Foundation Classes. Automation in Construction 96, 554 – 566. doi:https://doi.org/10.1016/j.autcon.2018.10.014.

[49] Uggla, G., Horemuz, M., 2018b. Georeferencing Methods for IFC, in: Proceedings of the 2018 Baltic Geodetic Congress, BGC–Geomatics 2018, Institute of Electrical and Electronics Engineers Inc.. pp. 207–211. doi:10.1109/BGC-Geomatics.2018.00045.

[50] Wunderlich, T., Blankenbach, J., 2017. Building Information Modeling (BIM) und Absteckung [Building Information Modeling (BIM) and Setting-out], in: Ingenieurvermessung 2017, TU Graz. URL: http://mediatum.ub.tum.de/doc/1435852/1435852.pdf. accessed: 2020-03-29, [in German].

[51] Yin, X., Liu, H., Chen, Y., Al-Hussein, M., 2019. Building information modelling for off-site construction: Review and future directions. Automation in Construction 101, 72 – 91. doi:10.1016/j.autcon.2019.01.010.